Journal of Computational Physics 228 (2009) 2874–2905

Contents lists available at ScienceDirect

Journal of Computational Physics

journal homepage: www.elsevier.com/locate/jcp

On the time-splitting scheme used in the Princeton Ocean Model

V.M. Kamenkovich, D.A. Nechaev *

The University of Southern Mississippi, Department of Marine Science, 1020 Balch Blvd., Stennis Space Center, MS 39529, United States

ARTICLE INFO

Article history:
Received 17 January 2008
Received in revised form 9 December 2008
Accepted 22 December 2008
Available online 9 January 2009

PACS:
65M12
86A05

Keywords:
Ocean circulation models
Barotropic–baroclinic splitting
Time-stepping

ABSTRACT

The analysis of the time-splitting procedure implemented in the Princeton Ocean Model (POM) is presented. The time-splitting procedure uses different time steps to describe the evolution of interacting fast and slow propagating modes. In the general case the exact separation of the fast and slow modes is not possible. The main idea of the analyzed procedure is to split the system of primitive equations into two systems of equations for interacting external and internal modes. By definition, the internal mode varies slowly and the crux of the problem is to determine the proper filter, which excludes the fast component of the external mode variables in the relevant equations. The objective of this paper is to examine properties of the POM time-splitting procedure applied to equations governing the simplest linear non-rotating two-layer model of constant depth. The simplicity of the model makes it possible to study these properties analytically. First, the time-split system of differential equations is examined for two types of the determination of the slow component based on an asymptotic approach or time-averaging. Second, the differential-difference scheme is developed and some criteria of its stability are discussed for centered, forward, or backward time-averaging of the external mode variables. Finally, the stability of the POM time-splitting schemes with centered and forward time-averaging is analyzed. The effect of the Asselin filter on solutions of the considered schemes is studied. It is assumed that questions arising in the analysis of the simplest model are inherent in the general model as well.

© 2009 Elsevier Inc. All rights reserved.

1. Introduction

It is well known that perturbations in the ocean propagate with substantially different speeds. The phase speed of the fastest propagating perturbation imposes a restriction on time steps used in the *explicit* finite-difference models of the ocean circulation. Therefore, for the construction of an efficient explicit finite-difference scheme, one needs to somehow separate fast and slow processes so as to not solve for all governing equations at the time step dictated by the fastest propagating perturbation. This procedure is conventionally referred to as *time-splitting* and is utilized in many community Ocean General Circulation Models (OGCMs). In the case of linear equations and constant ocean depth the time-splitting problem is easily solved. A linear transformation of the variables allows us to split the initial problem into separate problems describing the propagation of barotropic and baroclinic modes of the considered motion. It is important that each of these modes propagates with a single phase speed and does not interact with other modes. Thus the choice of time step depends on the mode considered. In the general nonlinear viscous case with variable ocean depth these modes interact with each other and the exact mode separation becomes impossible.

* Corresponding author.
E-mail address: Vladimir.Kamenkovich@usm.edu (D.A. Nechaev).

0021-9991/$ - see front matter © 2009 Elsevier Inc. All rights reserved.
doi:10.1016/j.jcp.2008.12.033

Guided by the analysis of a constant depth linear model, one usually splits the system of primitive equations of the free-surface quasi-static OGCM into two systems of equations for external and internal modes. The depth-integrated horizontal velocity and sea-surface height are considered as external mode variables while the *slow* components of the 3D-velocity vector, temperature and salinity are considered as internal mode variables. The external mode is governed by the depth-integrated horizontal momentum and continuity equations, in which such variables as 3D-velocity vector, temperature, and salinity are considered as internal variables. The internal mode is governed by the system of primitive equations, in which only the slow components of depth-integrated horizontal velocities and sea-surface height are retained. In general, the solutions of both systems are interacting with each other but the separation can be accomplished at either every or multiple time steps. Such an approach makes it possible to use different time steps, resulting in the substantial increase in effectiveness of the finite-difference scheme as compared to the straightforward approach with one time step for all equations.

In general, the problem of separating fast and slow modes of motion has an asymptotic character. The primitive equations contain a small parameter equal to the ratio of typical speeds of propagation of slow and fast modes. While studying the fast mode asymptotically, the slow mode can be considered as time independent on some time interval. It implies that the external mode will depend parametrically on the internal mode on this time interval. The slow component of the external mode, which is to be used in the equations for the internal mode, can be revealed by filtering out the fast component. This is the main idea of the mode separation or time-splitting procedure. Essentially, the idea is implemented in many numerical models of the general ocean circulation and coastal dynamics, although the implementation depends on specifics of each model. See, for example, [4], [9, Chapter 9.5], [7] and references given therein.

Originally the time-splitting procedure used in the Princeton Ocean Model (POM) (see [3,11]) was suggested on an heuristic level based on some qualitative considerations. To analyze the POM procedure quantitatively we apply it to the simplest hydrodynamical model, having free waves with substantially different phase speeds. Based on the POM time-splitting procedure, we formulated two finite-difference schemes, which will be referred to as POM time-splitting schemes with centered and forward time-averaging. Our goal is to analyze properties of these schemes. As far as we know, this is the first attempt of such a kind. So consider the linear two-layer model with constant depth. Such a model has been widely used in the physical oceanography as a pilot model. It is helpful that in this case the exact solution of the system of differential equations of this model is easily found and can be used for the comparison with approximate solutions. First, we will study the time-splitting problem for differential equations of the model. We will formulate two types of the time-split system of differential equations based on different definitions of slow components of the external mode. Then we will examine the solutions of these systems and compare them with the exact solutions to find the conditions of their applicability. Second, we will analyze the stability of the formulated POM time-splitting schemes. By and large this study is similar to the analysis of finite-difference schemes approximating two-layer isopycnal-coordinate models performed by Higdon and Bennett [8], Hallberg [5] and Higdon [6], but it differs substantially in many respects. We assume that questions arising in the analysis of the simplest model are inherent in the general model as well.

Section 2 of the paper describes the basic equations of the model considered. In Section 3 the general solution of the system of differential equations of the model is given. Section 4 provides the analysis of the solution of the proper initial-value problem for small values of the ratio of speeds of slow and fast propagating perturbations. In Section 5 POM time-splitting schemes with centered and forward time-averaging are formulated. The asymptotic analysis of the time-split system of differential equations is presented in Section 6. The effect of time-averaging of the external mode in the equations describing the evolution of the internal mode is discussed in Section 7. Section 8 describes the results of the stability analysis of the corresponding differential-difference problems, useful when the ratio of internal and external time steps is large. Section 9 presents the stability analysis of the POM time-splitting schemes, formulated in Section 5. Section 10 outlines the conclusions.

2. Basic equations

Consider a linear two-layer non-rotating and non-viscous ocean model of constant depth under the Boussinesq approximation. The momentum and continuity equations for the upper and lower layers are as follows:

$$\frac{\partial u_1}{\partial t} = -g\frac{\partial \eta}{\partial x}, \tag{1}$$

$$\frac{\partial}{\partial t}(\eta - \zeta) + \frac{\partial}{\partial x}(H_1 u_1) = 0, \tag{2}$$

$$\frac{\partial u_2}{\partial t} = -g\frac{\partial}{\partial x}(\eta + \varepsilon\zeta), \tag{3}$$

$$\frac{\partial \zeta}{\partial t} + \frac{\partial}{\partial x}(H_2 u_2) = 0, \tag{4}$$

where x is the spatial coordinate; t is time; u_1, ρ_1, H_1 and u_2, ρ_2, H_2 are the horizontal velocities, densities and undisturbed thicknesses of the upper and lower layers, respectively; η is sea-surface height; ζ is the interface perturbation; g is gravity; $\varepsilon = (\rho_2 - \rho_1)/\rho_0$, where ρ_0 is mean density.

For the subsequent separation of the external and internal modes, it is convenient to introduce the depth-averaged velocity u_a,

$$u_a = \frac{H_1}{H}u_1 + \frac{H_2}{H}u_2, \quad H = H_1 + H_2, \tag{5}$$

where H is the total depth, and to rewrite the system (1)–(4) as

$$\frac{\partial u_a}{\partial t} = -g\left(\frac{\partial \eta}{\partial x} + \varepsilon\frac{H_2}{H}\frac{\partial \zeta}{\partial x}\right), \tag{6}$$

$$\frac{\partial \eta}{\partial t} + \frac{\partial}{\partial x}(Hu_a) = 0, \tag{7}$$

$$\frac{\partial u_1}{\partial t} = -g\frac{\partial \eta}{\partial x}, \tag{8}$$

$$\frac{\partial \zeta}{\partial t} + \frac{\partial}{\partial x}(Hu_a - H_1u_1) = 0. \tag{9}$$

After solving system (6)–(9) for u_a, η, u_1, ζ we find u_2 from (5).

Eqs. (6) and (7) are the depth-integrated momentum and continuity equations (for the sake of convenience (6) is divided by H); Eq. (8) is the momentum equation for the upper layer; and Eq. (9) is the continuity equation for the lower layer. To further simplify the problem we will consider an x-periodic solution of (6)–(9) by assuming that

$$(u_a, \eta, u_1, \zeta) = Re\{(\tilde{u_a}, \tilde{\eta}, \tilde{u_1}, \tilde{\zeta})e^{ikx}\}, \tag{10}$$

where $\tilde{u_a}, \tilde{\eta}, \tilde{u_1}, \tilde{\zeta}$ are complex-valued amplitudes which depend only on t; k is the wave number; and Re implies the real part of the complex expression. Substituting (10) into (6)–(9) and omitting for brevity tildes over u_a, η, u_1, ζ gives

$$\frac{du_a}{dt} = -ikg\left(\eta + \varepsilon\frac{H_2}{H}\zeta\right), \tag{11}$$

$$\frac{d\eta}{dt} + ikHu_a = 0, \tag{12}$$

$$\frac{du_1}{dt} = -ikg\eta, \tag{13}$$

$$\frac{d\zeta}{dt} + ik(Hu_a - H_1u_1) = 0. \tag{14}$$

Consider also the case when x-derivatives in (6)–(9) are approximated by finite-difference ratios. Introduce a spatial grid with spacing Δx and define η and ζ at points $j\Delta x$ and velocities u_a and u_1 at points $(j+\frac{1}{2})\Delta x$, where j is an integer. Then by considering an x-periodical solution of the form

$$(u_a, u_1) = Re\left\{(\tilde{u_a}, \tilde{u_1})\exp\left[ik\left(j+\frac{1}{2}\right)\Delta x\right]\right\}, \quad (\eta, \zeta) = Re\{(\tilde{\eta}, \tilde{\zeta})\exp(ikj\Delta x)\}, \tag{15}$$

we end up with the same Eqs. (11)–(14) for amplitudes $\tilde{u_a}, \tilde{\eta}, \tilde{u_1}, \tilde{\zeta}$ but with k replaced with $k^* = (2/\Delta x)\sin(k\Delta x/2)$, where $0 < k\Delta x < \pi$.

In what follows, we restrict ourselves to the consideration of perturbations with a fixed wave number. A change of k can always be taken into account by rescaling t, therefore the magnitude of k will not influence the results of our analysis.

It is not difficult to show that the energy, defined as $H_1|u_1|^2 + H_2|u_2|^2 + g|\eta|^2 + g\varepsilon|\zeta|^2$, will be conserved following Eqs. (11)–(14). Note that in this expression u_2 should be replaced with u_a by using (5).

3. General solution of model equations

Mathematically (11)–(14) is the system of ordinary differential equations with constant coefficients so it is easy to write down the general solution of this system. Assuming that the sought functions are proportional to $e^{i\omega t}$ yields the characteristic equation for ω,

$$\omega^4 - gk^2(H + \varepsilon H_2)\omega^2 + g^2k^4\varepsilon H_1H_2 = 0. \tag{16}$$

Solving (16) for ω^2 gives

$$\omega_{1,2}^2 = \frac{gk^2}{2}\left[H + \varepsilon H_2 \pm \sqrt{(H+\varepsilon H_2)^2 - 4\varepsilon H_1H_2}\right]. \tag{17}$$

We see that all four roots $\pm\omega_1, \pm\omega_2$ of biquadratic equation (16) are real. Thus we have four waves traveling with phase velocities $\pm\omega_1/k, \pm\omega_2/k$. The general solution of the system (11)–(14) can be written in the form

$$u_a = -\frac{\omega_1}{Hk}(Ae^{i\omega_1 t} - Be^{-i\omega_1 t}) + \frac{\omega_2^3}{Hk(gH_1k^2 - \omega_2^2)}(Ce^{i\omega_2 t} - De^{-i\omega_2 t}), \tag{18}$$

$$\eta = Ae^{i\omega_1 t} + Be^{-i\omega_1 t} - \frac{\omega_2^2}{gH_1k^2 - \omega_2^2}(Ce^{i\omega_2 t} + De^{-i\omega_2 t}), \tag{19}$$

$$u_1 = -\frac{gk}{\omega_1}(Ae^{i\omega_1 t} - Be^{-i\omega_1 t}) + \frac{gk\omega_2}{gH_1k^2 - \omega_2^2}(Ce^{i\omega_2 t} - De^{-i\omega_2 t}), \tag{20}$$

$$\zeta = -\frac{gH_1k^2 - \omega_1^2}{\omega_1^2}(Ae^{i\omega_1 t} + Be^{-i\omega_1 t}) + Ce^{i\omega_2 t} + De^{-i\omega_2 t}, \tag{21}$$

where constants A, B, C, and D are arbitrary. They are determined from the specified initial values $u_a(0)$, $\eta(0)$, $u_1(0)$, and $\zeta(0)$. We see that for a rather broad range of ε the ratio ω_2/ω_1 is small (Fig. 1, the left panels). Using the upper indices f and s to indicate the fast (terms with frequency ω_1) and slow (terms with frequency ω_2) components, respectively, we find that any solution of (11)–(14) can be represented as

$$u_a = u_a^f + u_a^s, \quad \eta = \eta^f + \eta^s, \quad u_1 = u_1^f + u_1^s, \quad \zeta = \zeta^f + \zeta^s. \tag{22}$$

The same representation is true for u_2 (see Eq. (5)). Any solution of (11)–(14) can be considered as a 4D-vector (u_a, η, u_1, ζ). The fast component $(u_a^f, \eta^f, u_1^f, \zeta^f)$ of this vector is called the barotropic mode (or solution) while the slow component $(u_a^s, \eta^s, u_1^s, \zeta^s)$ is called the baroclinic mode (or solution) (see (22)). Note that the barotropic mode does not depend on the stratification for very small values of ε (see Section 5). This limit expression can be obtained directly from (11)–(14) by setting $\varepsilon = 0$ in (11). The expression of the baroclinic mode for very small values of ε can be obtained directly from (11)–(14) by deleting $d\eta/dt$ in (12) (the rigid lid approximation).

A different terminology is useful for the analysis of the POM time-splitting procedure. The procedure suggests that one considers two separate systems of Eqs. (11), (12) and (13), (14), respectively, with ζ in (11) replaced with ζ^s and η and u_a in (13) and (14) replaced with η^s and u_a^s. The solutions of these systems (η, u_a) and (ζ, u_1) are called external and internal modes, respectively. In contrast to the barotropic and baroclinic modes, the external and internal modes are 2D vectors.

It is helpful to compare the sea-surface elevation η and depth-averaged velocity u_a of the barotropic mode with the external mode and the interface ζ and velocity in the upper layer u_1 of the baroclinic mode with the internal mode. The external mode $[\eta = \eta^f + \eta^s;\ u_a = u_a^f + u_a^s]$ contains the slow component which is why the sea-surface elevation and depth-averaged velocity of the external mode *differ* from the sea-surface elevation and depth-averaged velocity (η^f, u_a^f) of the barotropic mode. This fact is well known (see, for example, Killworth et al. [10] who state: '...the depth-integrated flow is not precisely

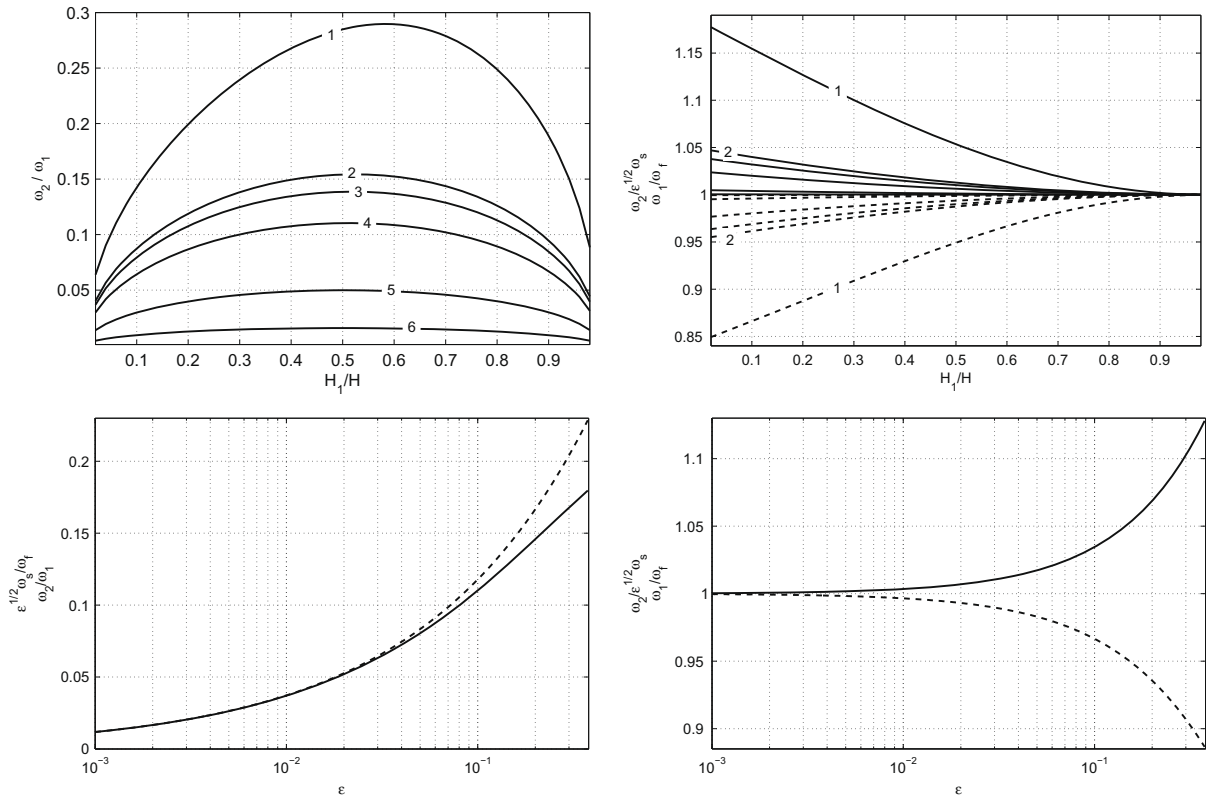

Fig. 1. The upper left panel: ω_2/ω_1 as a function of H_1/H. The curves: 1 – for $\varepsilon = 0.4$; 2 – $\varepsilon = 0.1$; 3 – $\varepsilon = 0.08$; 4 – $\varepsilon = 0.05$; 6 – $\varepsilon = 0.01$. The upper right panel: ω_1/ω_f (solid lines) and $\omega_2/(\varepsilon^{1/2}\omega_s)$ (dashed lines) as functions of H_1/H are shown for the same set of ε values: 1 – $\varepsilon = 0.4$; 2 – $\varepsilon = 0.1$ and so on. ω_1/ω_f and $(\omega_2/\varepsilon^{1/2}\omega_s)$ tend to unity when ε approaches zero. The lower left panel: ω_2/ω_1 (solid line) and $(\varepsilon^{1/2}\omega_s)/\omega_f$ (dashed line) as functions of ε for $H_1/H = 1/6$. The lower right panel: ω_1/ω_f (solid line) and $\omega_2/(\varepsilon^{1/2}\omega_s)$ (dashed line) as functions of ε for $H_1/H = 1/6, g = 9.8\ \mathrm{m/s^2}$.

the barotropic mode.'). The internal mode contains the slow component only ($\zeta = \zeta^s; u_1 = u_1^s$) which is why the interface and velocity in the upper layer of the internal mode *coincide* with the interface and velocity of the upper layer (ζ^s, u_1^s) of the baroclinic mode. It is appropriate to stress here that Eqs. (11) and (12) for the external mode are depth-integrated momentum and continuity equations, respectively.

4. Analysis of the initial-value problem at small ε values

The following formulas are needed for further comparisons. Suppose that ε is very small which is typical for the deep ocean. Expanding ω_1 and ω_2 into series in ε yields

$$\omega_1 = \omega_f\left[1 + \varepsilon\frac{H_2^2}{2H^2} + O(\varepsilon^2)\right], \tag{23}$$

$$\omega_2 = \varepsilon^{1/2}\omega_s\left[1 - \varepsilon\frac{H_2^2}{2H^2} + O(\varepsilon^2)\right], \tag{24}$$

where

$$\omega_f = \sqrt{gH}k, \quad \omega_s = \sqrt{\frac{gH_1H_2}{H}}k. \tag{25}$$

We see that $\frac{\omega_2}{\omega_1} = O(\varepsilon^{1/2})$, so ε will be the basic small parameter of our asymptotic problem (see qualitative description of the problem in Section 1).

Usually for the deep ocean it is assumed that ε is on the order of 10^{-3}. At such ε the slow frequency ω_2 is two orders of magnitude smaller than the fast frequency ω_1. For the subsequent analysis of the validity of some approximations we need to expand the exact solution (18)–(21) into series in ε. To do so, we need first to find the corresponding expansions for A, B, C, D. Consider the typical solution for the deep ocean for which $u_1^f = u_2^f = u_a^f = O(1)$ and $u_1^s \sim u_2^s$ but $u_a^s = o(1)$. Scalings for η and ζ follow from system (11)–(14). In fact, according to (11) $\eta + \varepsilon(H_2/H)\zeta$ is also $o(1)$. The slow component of u_1 is on the same order as the fast one. Then, because for the slow mode $\partial/\partial t = O(\varepsilon^{1/2})$, the slow component of η will be on the order of $O(\varepsilon^{1/2})$ and therefore the slow component of ζ will be $O(\varepsilon^{-1/2})$. It is clear that the fast and slow components of η and ζ are $O(1)$. Thus, the initial values $u_a(0), \eta(0), u_1(0)$ and $\zeta(0)$ are on the order of $O(1), O(1), O(1)$, and $O(\varepsilon^{-1/2})$, respectively. Putting $t = 0$ in (18)–(21), solving the resulting equations for A, B, C, and D and expanding them into series in ε gives

$$A = A_0 + \varepsilon^{1/2}A_1 + O(\varepsilon), \quad B = B_0 + \varepsilon^{1/2}B_1 + O(\varepsilon), \tag{26}$$

$$C = \varepsilon^{-1/2}C_{-1} + C_0 + \varepsilon^{1/2}C_1 + O(\varepsilon), \quad D = \varepsilon^{-1/2}D_{-1} + D_0 + \varepsilon^{1/2}D_1 + O(\varepsilon), \tag{27}$$

where all coefficients $A_0, A_1, B_0, B_1, C_{-1}, C_0, C_1, D_{-1}, D_0, D_1, \ldots$ in (26) and (27) do not depend on ε. Expansions in ε of fast and slow components of u_a, η, u_1, ζ are given in Appendix A (see (A.1)–(A.10)).

Note that we will not limit our analysis to very small values of ε. We extend the range of admissible ε up to 0.4 to study the behavior of the solution for the range of ε, where ω_2 is at least one order of magnitude smaller than ω_1. Such ε could be typical for some motions characterized by the entrainment of water of substantially different density. Fig. 1 provides the ratio ω_2/ω_1 along with normalized ω_1 and ω_2 as functions of H_1/H and ε ($10^{-3} < \varepsilon < 4 \cdot 10^{-1}$).

5. POM finite-difference schemes for solving model equations

As applied to the system of Eqs. (11)–(14), the POM time-splitting procedure can be realized in the following way. Fig. 2 shows the time grids for the external and internal mode equations with time steps Δt_e and Δt_i, respectively, and explains the

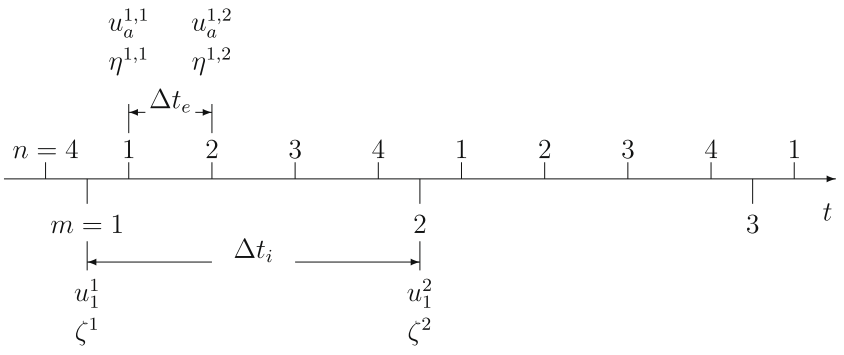

Fig. 2. The layout of the external and internal modes time grids with time steps Δt_e and $\Delta t_i = N\Delta t_e$ along with the appropriate mode variables for $N = 4$.

meaning of upper indices for variables u_a, η, u_1 and ζ. Suppose that variables $u_a^{0,N}, \eta^{0,N}, u_a^{1,1}$ and $\eta^{1,1}$ and variables u_1^1, ζ^1, u_1^2 and ζ^2 at two consecutive time steps are known. Then the finite-difference equations for $u_a^{m,n}$ and $\eta^{m,n}$,

$$\frac{u_a^{m,2} - u_a^{m-1,N}}{2\Delta t_e} = -ikg\left(\eta^{m,1} + \varepsilon\frac{H_2}{H}\zeta^m\right), \tag{28}$$

$$\frac{\eta^{m,2} - \eta^{m-1,N}}{2\Delta t_e} = -ikHu_a^{m,1}, \tag{29}$$

$$\frac{u_a^{m,3} - u_a^{m,1}}{2\Delta t_e} = -ikg\left(\eta^{m,2} + \varepsilon\frac{H_2}{H}\zeta^m\right), \tag{30}$$

$$\frac{\eta^{m,3} - \eta^{m,1}}{2\Delta t_e} = -ikHu_a^{m,2}, \tag{31}$$

$$\cdots$$

$$\frac{u_a^{m+1,1} - u_a^{m,N-1}}{2\Delta t_e} = -ikg\left(\eta^{m,N} + \varepsilon\frac{H_2}{H}\zeta^m\right), \tag{32}$$

$$\frac{\eta^{m+1,1} - \eta^{m,N-1}}{2\Delta t_e} = -ikHu_a^{m,N} \tag{33}$$

are integrated for $m = 1$. The values of $u_a^{1,n}$ and $\eta^{1,n}$ for $n = 1, \ldots, N$ are used to compute time averaged variables $\langle u_a\rangle^{1+\frac{1}{2}}$ and $\langle\eta\rangle^{1+\frac{1}{2}}$ from the following formulas:

$$\langle u_a\rangle^{m+\frac{1}{2}} = \frac{1}{N}\sum_1^N u_a^{m,n}, \quad \langle\eta\rangle^{m+\frac{1}{2}} = \frac{1}{N}\sum_1^N \eta^{m,n}, \ \ m = 1, 2, \ldots. \tag{34}$$

The integration of Eqs. (28)–(33) is then repeated for $m = 2$ to find $\langle u_a\rangle^{2+\frac{1}{2}}$ and $\langle\eta\rangle^{2+\frac{1}{2}}$ from (34). Finally, the time-stepping is performed to compute variables u_1^{m+1} and ζ^{m+1},

$$\frac{u_1^{m+1} - u_1^{m-1}}{2\Delta t_i} = -ikg\left[\frac{1}{2}\left(\langle\eta\rangle^{m-\frac{1}{2}} + \langle\eta\rangle^{m+\frac{1}{2}}\right)\right], \tag{35}$$

$$\frac{\zeta^{m+1} - \zeta^{m-1}}{2\Delta t_i} = -ik\left[H\frac{1}{2}\left(\langle u_a\rangle^{m-\frac{1}{2}} + \langle u_a\rangle^{m+\frac{1}{2}}\right) - H_1u_1^m\right] \tag{36}$$

for $m = 2$ and so on. Note that in the practical application of this scheme $\langle u_a\rangle^{m-\frac{1}{2}}$ and $\langle\eta\rangle^{m-\frac{1}{2}}$ are calculated at the previous time step and the recalculation of $u_a^{m-1,n}$ and $\eta^{m-1,n}, n = 2, \ldots, N$ is not required.

We interpret $u_a^{m,n}$ and $\eta^{m,n}$ as the *external* mode and u_1^m and ζ^m as the *internal* mode variables (see Section 3). We see that the external and internal modes interact at each time step Δt_i. The centered time-averaging over time interval $t_i - \Delta t_i, t_i + \Delta t_i$ is introduced to filter out the fast component of external mode variables $u_a^{m,n}$ and $\eta^{m,n}$ in Eqs. (35) and (36). The necessary condition of stability of the finite-difference scheme requires that $\omega_1\Delta t_e < 1$ and $\omega_2\Delta t_i < 1$. Notice that in the standard (without time-splitting) approach to the finite-difference approximation of (11)–(14) we have to use the time step Δt_e in all equations.

According to (A.1)–(A.10) the fast component of ζ is negligible as compared to the slow one. Therefore for describing ζ we can use the internal time step Δt_i, which is substantially greater than the external time step Δt_e for the description of u_a and η. Assuming that ζ is constant on the time step Δt_i, we find from system (11), (12) the external mode u_a and η, depending on ζ parametrically on this time step. Because the fast component of u_1 is equal to the fast component of u_a (their difference is on the order of $O(\varepsilon)$), we are seeking the slow component of u_1 only. Inserting the slow component of u_a and η in system (13), (14), we find the slow components of u_1 and ζ by using the time step Δt_i. For the general OGCM these estimates appear to be hypotheses that do not contradict overall concepts.

Based on results by Higdon and Bennett [8] on similar problems, we anticipate that the time-splitting finite-difference scheme (28)–(36) can be weakly unstable for parameters characteristic for the deep ocean. Fig. 3 presents results of integration of (28)–(36) for $\omega_1\Delta t_e = 0.01, \omega_1\Delta t_i = 0.1 (N = 10)$, and $\varepsilon = 5\cdot 10^{-3}$. To estimate the level of dissipation required to suppress instability of the time-splitting scheme, we included linear Newtonian friction with coefficient r to the momentum equations in the upper and lower layers of the two-layer model and conducted a set of forward runs for r in the range $[0, 10^{-3}/\Delta t_e]$. Curve 1 in Fig. 3 shows the energy amplification factor λ computed after integration of the initial-value problem for frictionally modified (28)–(36) over the time period $T = 60\pi/\omega_2$. The energy amplification factor is computed as a ratio of the energy of the solution (introduced at the end of Section 2) at times T and $T/2$ raised to the power $1/K$, where $K = T/2\Delta t_i$. Similar characteristics are computed for the scheme without time-splitting, which conserves energy for $r = 0$. Given the small Δt_e chosen for the experiment, the scheme without time-splitting reproduces the behavior of the analytical solution well. The amplification factor for this scheme as a function of r is shown by curve 3. As seen in Fig. 3 the price one has to pay for the efficiency of the time-splitting scheme is weak instability, which can be suppressed by the dissipation produced by the incorporated Newtonian friction with the coefficient $r = 10^{-3}/\Delta t_e$. It is useful to compare this friction with physically justified friction incorporated into the original POM model. We will consider the conventional quadratic bottom drag $c|\mathbf{u}|\mathbf{u}$, where the typical value for c is 0.0025 and $\mathbf{u}$ is the bottom velocity. It is reasonable to assume that the horizontal friction has

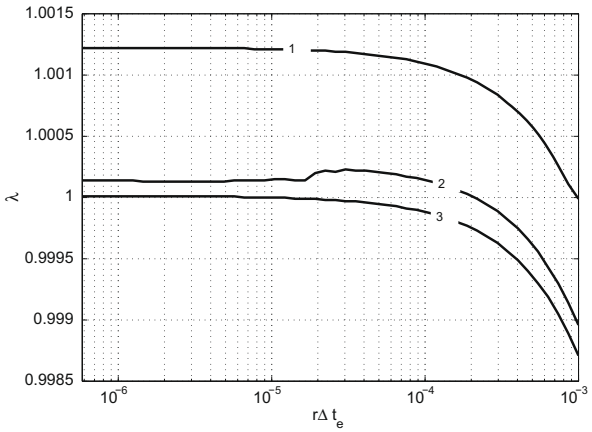

Fig. 3. Energy amplification factor λ as a function of the Newtonian friction coefficient r. Curve 1 represents the conventional POM time-splitting scheme with centered time-averaging; curve 2 represents the time-splitting scheme with forward time-averaging, and curve 3 represents the numerical scheme without time-splitting.

the same order of magnitude. The dissipation produced by the bottom friction is on the order of $c|\mathbf{u}|^3$ while the dissipation produced by the Newtonian friction is on the order of $rH|\mathbf{u}|^2$, where H is a typical depth of the model. The ratio of these two quantities is $c|\mathbf{u}|\Delta t_e/(10^{-3}H)$. The quantity $|\mathbf{u}|\Delta t_e$ does not depend on the choice of the time scale. Based on experimental practice with POM, we choose $\Delta t_e = 10$ s and $|\mathbf{u}| = 0.5$ m/s. Then the ratio is on the order of $12.5/H$. In most practical applications of POM typical H is certainly greater than 12.5 m. Thus we can argue that the Newtonian friction needed to completely suppress the weak instability in (28)–(36) could be excessive from the standpoint of physics. We need to keep in mind, however, that this instability may manifest itself during rather long time integration.

Along with the centered time-averaging utilized in the rhs of (35) and (36) we will use forward time-averaging, set up as

$$\frac{u_1^{m+1} - u_1^{m-1}}{2\Delta t_i} = -ikg\langle\eta\rangle^{m+\frac{1}{2}}, \tag{37}$$

$$\frac{\zeta^{m+1} - \zeta^{m-1}}{2\Delta t_i} = -ik(H\langle u_a\rangle^{m+\frac{1}{2}} - H_1 u_1^m). \tag{38}$$

Fig. 3, curve 2 shows that the scheme with forward time-averaging requires an order of magnitude smaller level of dissipation for stability. Note also that the investigation of the amplification factor is a very coarse proxy for the numerical stability analysis. The computed λ depends on initial conditions due to finite time interval of model integration. It is subject also to uncertainties due to truncation errors and due to the fact that for the non-energy conserving time-splitting schemes, the time evolution of energy is not necessarily monotonic.

In the remainder of the paper, we will refer to scheme (28)–(34); (35), (36) as the POM time-splitting scheme with centered time-averaging while to scheme (28)–(34); (37), (38) as the POM time-splitting scheme with forward time-averaging. Our goal is to study properties of these two POM time-splitting schemes. In the remainder of the paper we will not return to the consideration of the effect of the Newtonian friction on the stability of the schemes because the action of this friction is not time-scale dependent. Instead we consider the effect of the Asselin time filtering. As is known, the POM uses the Asselin filter [2] at every external and internal time steps to suppress the computational modes. The effect of this filter will be discussed in Sections 8 and 9.

6. Asymptotic interpretation of the POM time-splitting scheme

To examine the asymptotic solution of (11)–(14) for small ε values consider the following time-split system of differential equations:

$$\frac{du_a}{dt} = -ikg\left(\eta + \varepsilon\frac{H_2}{H}\zeta\right), \tag{39}$$

$$\frac{d\eta}{dt} + ikHu_a = 0, \tag{40}$$

$$\frac{du_1}{dt} = -ikg\eta^s, \tag{41}$$

$$\frac{d\zeta}{dt} + ik(Hu_a^s - H_1 u_1) = 0, \tag{42}$$

where the superscript s denotes the slow component.

According to (41) u_1 will contain the slow component only. Then in view of (42) ζ will also contain the slow component only and according to (A.8) $d\zeta^s/dt = O(1)$. Taking this into account we can easily find an approximate partial solution of (39), (40) as $u_a = 0, \eta = -\varepsilon(H_2/H)\zeta^s$. In fact, this solution satisfies (39) exactly and (40) with the accuracy of $O(\varepsilon)$. Thus the general solution of the system (39), (40) will be

$$u_a = \frac{\omega_f}{Hk}\left(\hat{a}e^{i\omega_f t} + \hat{b}e^{-i\omega_f t}\right), \tag{43}$$

$$\eta = \hat{a}e^{i\omega_f t} + \hat{b}e^{-i\omega_f t} - \varepsilon\frac{H_2}{H}\zeta^s, \tag{44}$$

where $\hat{a}$ and $\hat{b}$ are arbitrary constants. According to (43) and (44)

$$u_a^s = 0, \quad \eta^s = -\varepsilon\frac{H_2}{H}\zeta^s. \tag{45}$$

Now we consider system (41), (42). It takes the following form:

$$\frac{du_1^s}{dt} = \varepsilon ikg\frac{H_2}{H}\zeta^s, \tag{46}$$

$$\frac{d\zeta^s}{dt} = ikH_1u_1^s. \tag{47}$$

The general solution of this system is

$$u_1^s = \varepsilon^{1/2}\frac{\omega_s}{H_1k}\left(\bar{c}e^{i\omega_s\varepsilon^{1/2}t} - \bar{d}e^{-i\omega_s\varepsilon^{1/2}t}\right), \tag{48}$$

$$\zeta^s = \bar{c}e^{i\omega_s\varepsilon^{1/2}t} + \bar{d}e^{-i\omega_s\varepsilon^{1/2}t}, \tag{49}$$

where $\bar{c}$ and $\bar{d}$ are arbitrary constants. If assume that $u_1^s = O(1)$, then

$$\bar{c} = \varepsilon^{-1/2}\hat{c}_{-1}, \quad \bar{d} = \varepsilon^{-1/2}\hat{d}_{-1}. \tag{50}$$

The constants $\hat{a}, \hat{b}, \hat{c}_{-1}$ and $\hat{d}_{-1}$ do not depend on ε. The comparison with corresponding formulas from Appendix A shows that we indeed obtained the first approximation to u_a, η, u_1^s and ζ^s but under the condition that $\omega_f t = O(\varepsilon^{-1/2})$ (according to (A.9) $\varepsilon\omega_f t$ should be small). Note that $u_a^s = O(\varepsilon)$, so $u_a^s = 0$ is really the first approximation to u_a^s. Thus we see that the time-split system of Eqs. (39)–(42) gives the correct solution for the time interval on the order of slow mode period only.

The outlined approach is approximate because we did not strictly define what we imply by the slow mode in system (39)–(42). Based on the form of exact solution (A.1)–(A.8) we introduce times with different scales:

$$T_0 = t, \quad T_1 = \varepsilon^{1/2}t, \quad T_2 = \varepsilon t, \quad \ldots \tag{51}$$

and define the slow mode as the mode that does *not* depend on T_0. Thus we will seek the general solution of system (39)–(42) as

$$u_a = u_{(a)0}(T_0, T_1, T_2, \ldots) + \varepsilon^{1/2}u_{(a)1}(T_0, T_1, T_2, \ldots) + \cdots, \tag{52}$$

$$\eta = \eta_0(T_0, T_1, T_2, \ldots) + \varepsilon^{1/2}\eta_1(T_0, T_1, T_2, \ldots) + \cdots, \tag{53}$$

$$u_1 = u_{(1)0}(T_0, T_1, T_2, \ldots) + \varepsilon^{1/2}u_{(1)1}(T_0, T_1, T_2, \ldots) + \cdots, \tag{54}$$

$$\zeta = \varepsilon^{-1/2}\zeta_{-1}(T_0, T_1, T_2, \ldots) + \zeta_0(T_0, T_1, T_2, \ldots) + \varepsilon^{1/2}\zeta_1(T_0, T_1, T_2, \ldots) + \cdots, \tag{55}$$

where all functions in (52)–(55) are assumed bounded (compare with (A.1)–(A.8)). In Appendix B we provide the detailed asymptotic analysis of system (39)–(42) by applying the method of multiple time scales. The comparison with the corresponding terms in (A.1)–(A.10) shows that *all of the slow components of u_a, η, u_1 and ζ are determined correctly.* All fast components of u_1, ζ appear to be equal to zero and starting from $u_{(a)2}^f$ the fast component of u_a is in error. Recall that we decided not to determine the fast components of u_1, ζ. Thus only the first two approximations of the fast component of external mode on the time interval $\omega_f t = O(\varepsilon^{-1/2})$ are determined correctly. Note that the length of this time interval is on the order of the slow mode period. A similar conclusion follows from the comparison of the approximate solution (48), (49) with the exact solution (see Appendix A).

Formally system (39)–(42) differs from the original system (11)–(14). The question is what are the relationships between the solutions of these systems. In system (39)–(42), we used the asymptotic definition of slow components which is exact at small ε values. Thus we have shown that the time-split system of differential equations (39)–(42) describes correctly on large time intervals the slow components of u_a, η, u_1 and ζ only while the fast components of u_a, η, u_1 and ζ are described correctly on the time interval on the order of slow mode period.

It is worth noting that the fast component of ζ influence the fast components of u_a, η, starting from the third approximation. This conclusion by itself does not violate the condition of absence of the resonance in system (39), (40) on the frequency ω_f. The point is that this condition depends not only on approximations of ζ^f (see Appendix B).

7. Effect of time-averaging

Consider the system (39)–(42) using time-averaging to filter out the fast component from u_a and η in Eqs. (41) and (42). We will apply three types of time-averaging: centered, forward and backward. Correspondingly for η we have

$$\langle\eta\rangle_c = \frac{1}{T}\int_{t-\frac{T}{2}}^{t+\frac{T}{2}} \eta(\tau)d\tau, \quad \langle\eta\rangle_f = \frac{1}{T}\int_{t}^{t+T} \eta(\tau)d\tau, \quad \langle\eta\rangle_b = \frac{1}{T}\int_{t-T}^{t} \eta(\tau)d\tau, \tag{56}$$

where subscripts c, f, and b stand for centered, forward, and backward averaging, respectively, and T is the period of time-averaging. Similar relations will be applied for u_a. So we have

$$\frac{du_a}{dt} = -ikg\left(\eta + \varepsilon\frac{H_2}{H}\zeta\right), \tag{57}$$

$$\frac{d\eta}{dt} + ikHu_a = 0, \tag{58}$$

$$\frac{du_1}{dt} = -ikg\langle\eta\rangle, \tag{59}$$

$$\frac{d\zeta}{dt} + ik(H\langle u_a\rangle - H_1u_1) = 0, \tag{60}$$

where $\langle\cdots\rangle$ is one of the three types of averaging (56). The asymptotic definition of the slow components of u_a and η used in (41), (42) is difficult to realize in a practical application. Therefore, for the determination of slow components of u_a and η in (59) and (60) we use the time-averaging with some time period T. Notice that the considered time-averaging does not provide the slow components exactly but only with some approximation.

Let us look for the oscillatory solutions of (57)–(60) proportional to $e^{i\omega t}$. After some manipulation we obtain the following characteristic equation for ω:

$$\omega^4 - gk^2(H + \varepsilon H_2G)\omega^2 + g^2k^4\varepsilon H_1H_2G = 0, \tag{61}$$

where G is one of the following expression depending on the type of averaging,

$$G_c = \frac{2}{\omega T}\sin\left(\frac{\omega T}{2}\right), \quad G_f = \frac{1}{i\omega T}(e^{i\omega T} - 1), \quad G_b = \frac{1}{i\omega T}(1 - e^{-i\omega T}). \tag{62}$$

First, consider the centered time-averaging. Eq. (61) can be rewritten as

$$\frac{1}{g\varepsilon H_2k^2}\frac{\omega^4 - gHk^2\omega^2}{gH_1k^2 - \omega^2} = -G_c. \tag{63}$$

It is convenient to analyze (63) graphically (see Fig. 4). Let us start with small T. In this case G_c is close to one and we have two positive roots $\omega^{(1)}$ and $\omega^{(2)}, \omega^{(1)} > \omega^{(2)}$. The lhs of (63) is an even function of ω, so we will consider positive roots only. As T increases, the 'slow' root $\omega^{(2)}$ decreases and even secondary 'slow' roots $\omega^{(k)}, k = 3, \ldots$ of (63) appear, which are all less than the original $\omega^{(2)}$ for very small T (upper panel). Notice that no new 'fast' roots appear. The appearance of new slow roots is demonstrated in detail in Fig. 5. It is worth stressing that for a given T the secondary roots appear not for all ε. Note that, first, a multiple root appears and then it splits into two real roots while T is increasing. So we can conclude that no complex roots of (63) exist.

How do we choose T? As long as we have two positive roots of (63) only, we can uniquely solve the initial-value problem for (57)–(60). By representing the solution of (57)–(60) in the form (18)–(21) with the same constants A, B, C and D we see that for the fast oscillatory solution of (57)–(60) (frequency $\omega^{(1)}$) the amplitudes of u_a, η do not change while the amplitudes of u_1, ζ are multiplied by $G(\omega^{(1)}T)$, as compared to the amplitudes of (18)–(21). For the slow oscillatory solution of (57)–(60) (frequency $\omega^{(2)}$) the amplitudes of u_a, η are divided by $G(\omega^{(2)}T)$ while the amplitudes of u_1, ζ do not change. If we choose T such that $1/\omega^{(1)} \ll T \ll 1/\omega^{(2)}$, then $G(\omega^{(1)}T) \simeq 0$ and $G(\omega^{(2)}T) \simeq 1$. Thus, the fast oscillatory solution of (57)–(60) gives the correct fast component of u_a, η only while the slow oscillatory solution gives the correct slow components of all variables u_a, η, u_1 and ζ. This is sufficient to determine the external and internal modes. Such a choice is possible for $\varepsilon = 5 \cdot 10^{-3}$. In fact, taking T such that $\omega_fT = 10\pi(T/T_f = 5$, where $T_f = 2\pi/\omega_f)$ gives $\omega^{(1)}T = 3.1 \cdot 10$, $G_c(\omega^{(1)}T) = 1.3 \cdot 10^{-2}$ and $\omega^{(2)}T = 8.4 \cdot 10^{-1}$, $G_c(\omega^{(2)}T) = 9.7 \cdot 10^{-1}$. For $\varepsilon = 2 \cdot 10^{-1}$ we cannot choose a value of T that satisfies both conditions simultaneously. So for any choice of T we will modify either external or internal modes. It is worth stressing that sufficiently large T can generate secondary slow roots, in which case, the initial-value problem for (57)–(60) becomes non-unique. Thus, starting from some value of T, solutions of (57)–(60) are substantially distinct from the corresponding solutions of (11)–(14), although frequencies ω_1 and ω_2 still differ on the order of a magnitude.

At small ε we can introduce T depending on ε and find expansions of $\omega^{(1)}$ and $\omega^{(2)}$ in ε. It is possible to show that at relevant choices for T one can obtain the correct first approximation of our solution but on the bounded time interval only.

It is quite clear that there are no real roots of (61) for the forward and backward time-averaging. Let us start again with very small T and expand the roots of (61) into a series in T. We find that

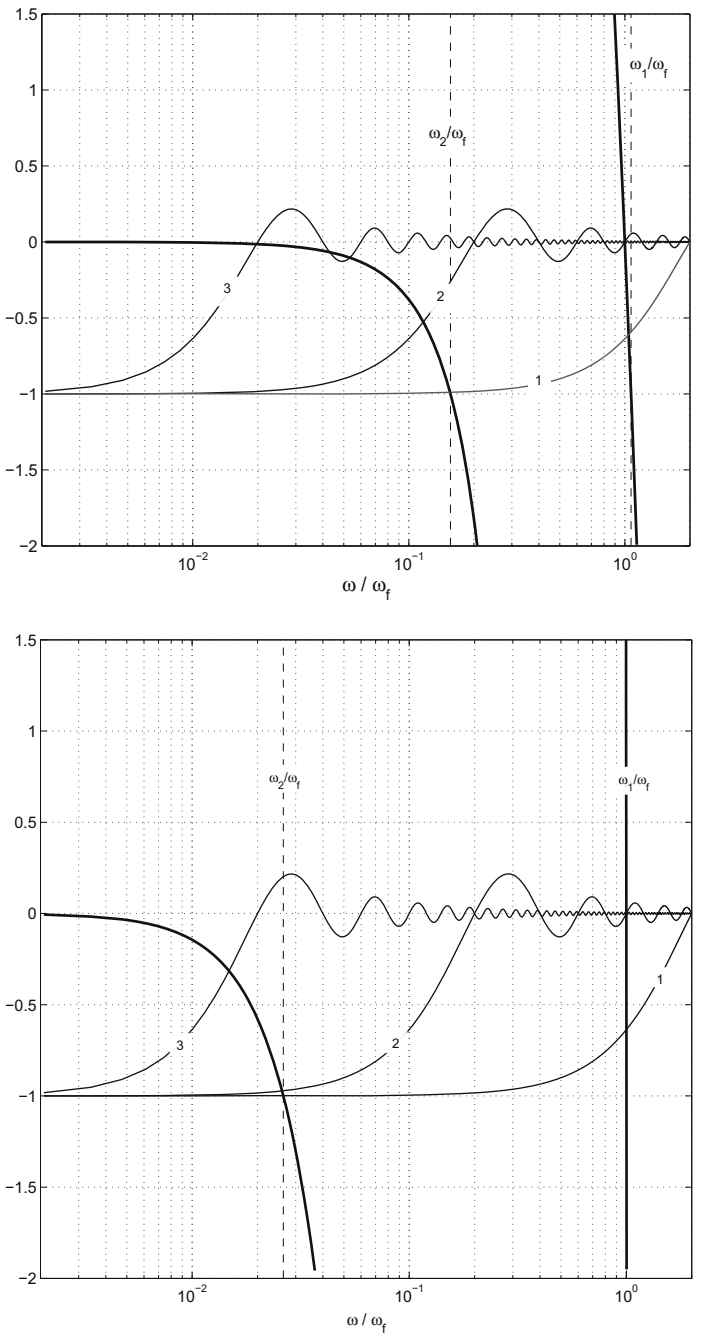

Fig. 4. This fugure shows how solutions of (63) are found. Bold solid lines represent the lhs of (63) computed for $\varepsilon = 2 \cdot 10^{-1}$ (upper panel) and $\varepsilon = 5 \cdot 10^{-3}$ (lower panel) as functions of ω/ω_f. Thinner solid lines (1,2,3) show rhs of (63) as functions of ω/ω_f computed for three values of $\omega_f T$: π for curve 1, 10π for curve 2, 100π for curve 3. Vertical dashed lines indicate the location of frequencies ω_1/ω_f and ω_2/ω_f. In the lower panel a segment of the bold line giving the 'fast' ω is practically vertical within the plot. $k = 2\pi \times 10^{-3}$ m^{-1} and $H_1/H = 1/6$ for all panels and subsequent considerations.

$$\omega_j(\varepsilon, T) = \omega_j(\varepsilon, 0) + a_j(\varepsilon)T + \cdots, \tag{64}$$

where

$$a_j(\varepsilon) = \mp \frac{\varepsilon H_2 \omega_j^2(\varepsilon,0)[gH_1k^2 - \omega_j^2(\varepsilon,0)]}{4[(H+\varepsilon H_2)\omega_j^2(\varepsilon,0) - 2g\varepsilon H_1 H_2 k^2]} i, \tag{65}$$

the minus (plus) signs stand for the forward (backward) time-averaging and $\omega_j(\varepsilon, 0)$ is one of the roots of (16). It is easy to check that for all roots of (16) $a_j(0) > 0$ in the case of forward averaging and $a_j(0) < 0$ in the case of backward averaging.

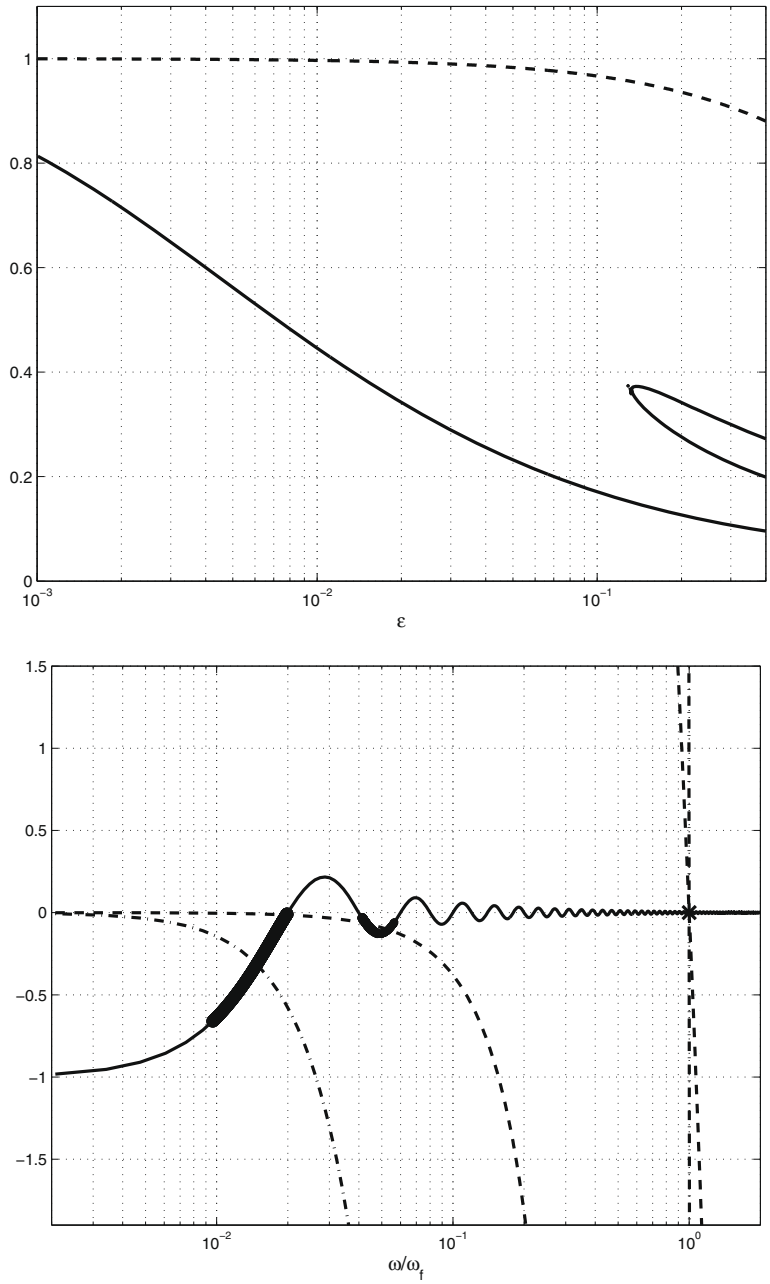

Fig. 5. The upper panel shows the roots of Eq. (63) for $\omega_f T = 100\pi$ as functions of ε, see Fig. 4. The dashed curve shows the 'fast' root $\omega^{(1)}$ of (63) normalized by ω_f. The solid curves show the 'slow' roots $\omega^{(2)}, \omega^{(3)}, \omega^{(4)}$ of (63) normalized by ω_f. The lower panel illustrates the origin of the multiple roots. The solid curve shows rhs of (63) for $\omega_f T = 100\pi$. The dashed curve gives lhs of (63) for $\varepsilon = 2 \cdot 10^{-1}$ and dashed-dotted curve shows lhs of (63) for $\varepsilon = 5 \cdot 10^{-3}$. Crosses denote the 'fast' roots of (63) for the range of $\varepsilon = [2 \cdot 10^{-3}, 4 \cdot 10^{-1}]$. Since the 'fast' roots exhibit slight variation with ε, these roots are seen as a single cross. Circles denote the intersections of curves giving the 'slow' roots of (63) for the same range of ε. Smaller circles show 'secondary' slow roots. These circles coalesce and appear as bold segments.

Therefore in the case of forward time-averaging, all roots $\omega_j(\varepsilon, T)$ shift to upper half-plane of complex ω for $T \neq 0$. These roots cannot return to the real axis, because (61) has no real roots for $T \neq 0$. Thus, for the forward time-averaging all oscillatory solutions of (57)–(60) will exponentially decay with time. In the case of backward time-averaging, all oscillatory solutions of (57)–(60) will exponentially grow. We did not try to determine the number of roots in these cases. Yet the conclusion on the choice of T made while considering the centered time-averaging holds in theses cases as well.

Note that system (57)–(60) does not conserve energy when time-averaging is applied ($T \neq 0$). Notice also that system (57)–(60) is formally the system of integral–differential equations. This fact can explain the non-uniqueness of the solution of the initial-value problem for some values of T.

8. Stability analysis of differential-difference system of model equations

Because $\Delta t_e \ll \Delta t_i$, examine the limit case when Δt_i is fixed and $\Delta t_e \to 0$ (or $N \to \infty$). In this case we can consider differential equations for the external mode and finite-difference equations for the internal mode. Suppose that u_1^1, ζ^1, u_1^2 and ζ^2 are specified. To determine u_1^3, ζ^3 we use the following system of finite-difference equations (approximating (59), (60)),

$$\frac{u_1^3 - u_1^1}{2\Delta t_i} = -ikg\langle\eta\rangle^2, \tag{66}$$

$$\frac{\zeta^3 - \zeta^1}{2\Delta t_i} + ik(H\langle u_a\rangle^2 - H_1 u_1^2) = 0, \tag{67}$$

where $\langle\ldots\rangle$ implies one of the three types of averaging (56). To find $\langle u_a\rangle_b^2$ and $\langle\eta\rangle_b^2$ we assume that ζ does not change on the time interval $(0, \Delta t_i)$ and consider (57), (58) with ζ replaced with ζ^1,

$$\frac{du_a}{dt} = -ikg\left(\eta + \varepsilon\frac{H_2}{H}\zeta^1\right), \tag{68}$$

$$\frac{d\eta}{dt} + ikHu_a = 0. \tag{69}$$

The solution of this system is found in Appendix C (see (C.1) and (C.2)). In line with the condition $N \gg 1$ we assume that,

$$\omega_f \Delta t_i \gg 1. \tag{70}$$

The point is that $\omega_f = 2\pi/T_f$ and the fast period T_f is proportional to Δt_e with a finite coefficient of proportionality. Averaging solution (C.1) and (C.2) over the time interval $(0, \Delta t_i)$ and using (C.5), (C.6) and (C.9) gives (in the limit when $\omega_f \Delta t_i$ tends to ∞)

$$\langle u_a\rangle_b^2 = 0, \quad \langle\eta\rangle_b^2 = -\varepsilon\frac{H_2}{H}\zeta^1. \tag{71}$$

At the time interval $(\Delta t_i, 2\Delta t_i)$ we suppose that $\zeta = \zeta^2$. Determining the solution of (57), (58) with ζ replaced with ζ^2, which satisfies the condition of continuity at $t = \Delta t_i$, gives (C.3), (C.4). Averaging this solution over the time interval $(\Delta t_i, 2\Delta t_i)$ and using (C.7)–(C.9) yields (in the limit when $\omega_f \Delta t_i$ tends to ∞)

$$\langle u_a\rangle_f^2 = 0, \quad \langle\eta\rangle_f^2 = -\varepsilon\frac{H_2}{H}\zeta^2. \tag{72}$$

The centered time-averaging is the mean value of backward and forward time-averaging. In the limit when $\omega_f \Delta t_i$ tends to ∞ we have

$$\langle u_a\rangle_c^2 = 0, \quad \langle\eta\rangle_c^2 = -\varepsilon\frac{H_2}{2H}(\zeta^1 + \zeta^2). \tag{73}$$

Consider the case of centered time-averaging. Substitution of (73) into (66) and (67) gives the system of finite-difference equations for determining u_1^3, ζ^3,

$$\frac{u_1^3 - u_1^1}{2\Delta t_i} = a(\zeta^1 + \zeta^2), \tag{74}$$

$$\frac{\zeta^3 - \zeta^1}{2\Delta t_i} + bu_1^2 = 0, \tag{75}$$

where

$$a = ikg\varepsilon\frac{H_2}{2H}, \quad b = -ikH_1. \tag{76}$$

The next step is to apply the Asselin filter to u_1^2, ζ^2 to obtain $\tilde{u}_1^2, \tilde{\zeta}^2$ [2]. For example,

$$\tilde{u}_1^2 = u_1^2 + \alpha(u_1^1 - 2u_1^2 + u_1^3) \tag{77}$$

and similarly for $\tilde{\zeta}^2$, where α is a parameter of the filter. By using (74) and (75), we exclude u_1^3 and ζ^3 from (77) and the similar expression for $\tilde{\zeta}^2$. We have

$$\tilde{u}_1^2 = 2\alpha u_1^1 + (1 - 2\alpha)u_1^2 + 2\Delta t_i a\alpha(\zeta^1 + \zeta^2), \tag{78}$$

$$\tilde{\zeta}^2 = 2\alpha\zeta^1 + (1 - 2\alpha)\zeta^2 + 2\Delta t_i b\alpha u_1^2. \tag{79}$$

The final step is to replace u_1^2, ζ^2 with $\tilde{u}_1^2, \tilde{\zeta}^2$. Thus we calculated $u_1^3, \zeta^3, \tilde{u}_1^2$ and $\tilde{\zeta}^2$ from the given u_1^2, ζ^2, u_1^1 and ζ^1. Analogously we will calculate $u_1^4, \zeta^4, \tilde{u}_1^3$ and $\tilde{\zeta}^3$ from the known $u_1^3, \zeta^3, \tilde{u}_1^2$ and $\tilde{\zeta}^2$ and so on. Introduce the 4D-vector ψ^m, which in the transposed form is

$$\psi^m = (u_1^{m+1}, \zeta^{m+1}, \tilde{u}_1^m, \tilde{\zeta}^m) \tag{80}$$

and set $\psi^1 = (u_1^2, \zeta^2, u_1^1, \zeta^1)$. Then relations of the type (74), (75), (78) and (79) can be written in the matrix form,

$$\boldsymbol{\psi}^{m+1} = M_c \boldsymbol{\psi}^m \quad \text{for } m = 1, \ldots \tag{81}$$

For the centered time-averaging the matrix M is

$$M_c = \begin{pmatrix} 0 & 2\Delta t_i a & 1 & 2\Delta t_i a \\ -b & 0 & 0 & 1 \\ 1-2\alpha & 2\Delta t_i a\alpha & 2\alpha & 2\Delta t_{ia}\alpha \\ 2\Delta t_i b\alpha & 1-2\alpha & 0 & 2\alpha \end{pmatrix}. \tag{82}$$

In the case of forward or backward time-averaging the relation similar to (81) is also true but matrix M_c should be replaced with appropriate matrices M_f or M_b. These matrices can be easily written out.

The considered scheme is stable if *all* eigenvalues λ of matrix M_c (M_f or M_b) are such that their moduli $|\lambda|$ are less than or equal to unity. Otherwise the scheme is unstable. We will start with the scheme without the Asselin filter ($\alpha = 0$). We will have three equations for eigenvalues λ:for the centered time-averaging,

$$\lambda^4 + (4\Delta t_i^2 ab - 2)\lambda^2 + 4\Delta t_i^2 ab\lambda + 1 = 0 \tag{83}$$

for the forward time-averaging,

$$\left(\lambda - \frac{1}{\lambda}\right)^2 = -4\Delta t_i^2 ab \tag{84}$$

for the backward time-averaging,

$$\lambda^4 - 2\lambda^2 + 4\Delta t_i^2 ab\lambda + 1 = 0, \tag{85}$$

where

$$ab = \varepsilon\omega_s^2 > 0. \tag{86}$$

These equations can be analyzed analytically. Let us start with (83) and denote the polynomial on the rhs of (83) by $P(\lambda)$. First of all we see that $\lambda_4 = -1$ is a root of this polynomial. Then $P'(-1) = -4\Delta t_i^2 ab$ and because $P(0) = 1$ we have another real root λ_3 that lies within interval $(-1, 0)$. Therefore $0 < \lambda_3\lambda_4 < 1$ and $\lambda_1\lambda_2$ will be greater than one. These roots will lie on the right half-plane of λ because according to (83) $\lambda_1 + \lambda_2 + \lambda_3 + \lambda_4 = 0$. Roots λ_1 and λ_2 will be complex conjugate. Otherwise, at least one of these roots will be greater than one which is impossible because $P(1) > 0$ and $P' = 4\lambda(\lambda^2 - 1) + 8\Delta t_i^2 ab\lambda + 4\Delta t_i^2 ab > 0$ for $\lambda \geqslant 1$. Roots λ_1 and λ_2 will always lie outside the unit circle $|\lambda| = 1$. If they hit this circle, then λ_4 and λ_3 coalesce at $\lambda = -1$ which is impossible because $P'(-1) \neq 0$. Thus, scheme (74), (75) with centered time-averaging is unstable for all Δt_i. Roots λ_3, λ_4 represent computational modes while roots λ_1, λ_2 represent physical modes. The physical modes correspond to oscillations with $\pm\varepsilon^{1/2}\omega_s$ frequencies. However, these modes will grow with time exponentially. Thus, the scheme (74), (75) with centered time-averaging is applicable only on the limited time interval (compare with Section 6).

It is worth noting that the discussed instability is not connected with a possible violation of the necessary condition of stability caused by incomplete filtering out of the fast component of u_a and η in (66), (67) ([8]; see also [5]). By assuming the validity of (70) we fully filtered out these fast components from $\langle u_a \rangle$ and $\langle \eta \rangle$ (see also a note at the end of Section 6).

If $\varepsilon^{1/2}\omega_s\Delta t_i < 1$, all roots of (84) lie on the unit circle $|\lambda| = 1$, two (λ_1 and λ_2) on the right half-plane (physical modes) and two (λ_3 and λ_4) on the left half-plane (computational modes). Thus, under this condition, scheme (66), (67) with forward time-averaging is stable. It is easy to show that λ_1^m will tend toward $\exp(i\varepsilon^{1/2}\omega_s t)$ if $\Delta t_i \to 0$ and $t = m\Delta t_i$ is fixed ($Im\{\lambda_1\} > 0$). It is possible that the stability of this scheme is connected with the fact that system (57)–(60) with forward time-averaging has exponentially decaying oscillatory solutions only, but there is no visible damping of the solution.

Let us finally turn to Eq. (85). Because $P(-1) = -4\Delta t_i^2 ab$ and $P(0) > 0$ two roots λ_3 and λ_4 are real and lie on the negative axis ($\lambda_3 > -1$ while $\lambda_4 < -1$). Consider a particular case when $4\Delta t_i^2 ab = 1$. In this case $\lambda_{1,2} = 1.0276 \pm 0.7366i$, $\lambda_3 = -0.3715$, $\lambda_4 = -1.6838$. Hence λ_1 and λ_2 lie outside the unit circle $|\lambda| = 1$. Now we can vary $4\Delta t_i^2 ab$ from $4\Delta t_i^2 ab = 1$ to any arbitrary value. As this takes place, the layout of roots, found for $4\Delta t_i^2 ab = 1$, will persist. Roots λ_1 and λ_2 cannot hit either the circle $|\lambda| = 1$ or the real axis at $\lambda \geqslant 1$. In the former, λ_3 and λ_4 will coalesce at $\lambda = -1$ which is impossible since $P'(-1) \neq 0$ for all $4\Delta t_i^2 ab \neq 0$. In the latter, $P(1) > 0$ and $P' = 4\lambda(\lambda^2 - 1) + 4\Delta t_i^2 ab > 0$ for all $\lambda \geqslant 1$. Thus, scheme (66), (67) with backward time-averaging is unstable for all Δt_i. Both physical modes will grow with time which also limits the time interval of applicability of this scheme.

For the graphical illustration of these results, we calculated eigenvalues λ of the appropriate matrices for two different Δt_i: $\omega_f\Delta t_i = 0.8\pi$ and $\omega_f\Delta t_i = 3.2\pi$ (Figs. 6–9). The first value has been chosen for the comparison with results of Section 9, although it is only marginally compatible with condition (70). The second value is compatible with condition (70). Note that it is impossible to distinguish between physical and computational roots in Fig. 7 after the corresponding curves intersect at points $(0, i)$ and $(0, -i)$. Notice also that analytical expressions for roots of (84) show that the bending of curves in the vicinity of $(0, i)$ and $(0, -i)$ is caused by the limited accuracy of computations. Actually these two curves intersect each other at right angle.

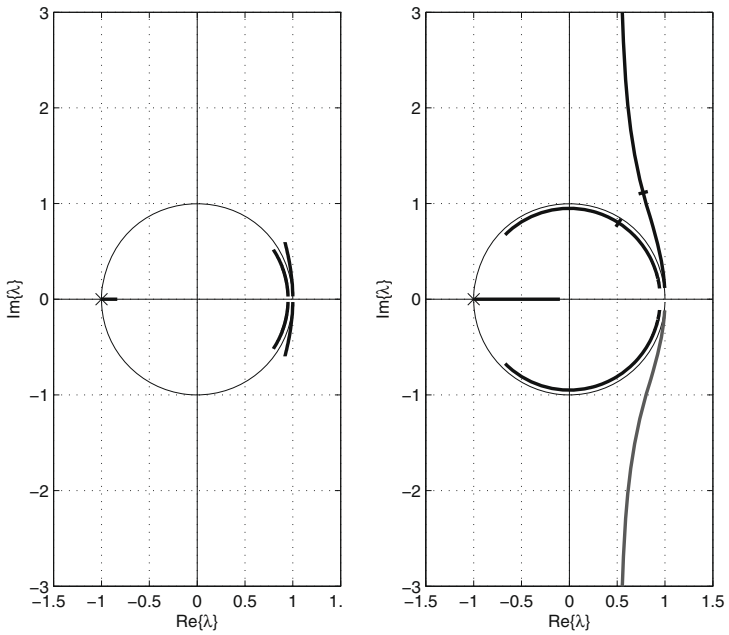

Fig. 6. The layout of eigenvalues of matrix M_c for $\alpha = 0$ (roots of Eq. (83)) for $\omega_f \Delta t_i = 0.8\pi$ (left panel) and $\omega_f \Delta t_i = 3.2\pi$ (right panel) for ε in the range $[1 \cdot 10^{-3}, 0.4]$. Eigenvalue curves are shown by bold lines. The computational λ lie on the left half-plane while the physical λ lie on the right half-plane. Eigenvalue $\lambda_4 = -1$, which is not changed with ε, is given by a cross. λ_3 is shown by the segment of the negative $R\{\lambda\}$-axis. Bold segments on the unit circle identify $\exp(\pm i\varepsilon^{1/2}\omega_s \Delta t_i)$ for the same range of ε. For clarity of the plot they are shifted to the interior of the circle $|\lambda| = 1$. For comparisons we put marks on some curves to divide portions, for which $\varepsilon^{1/2}\omega_s \Delta t_i$ is smaller or greater than unity.

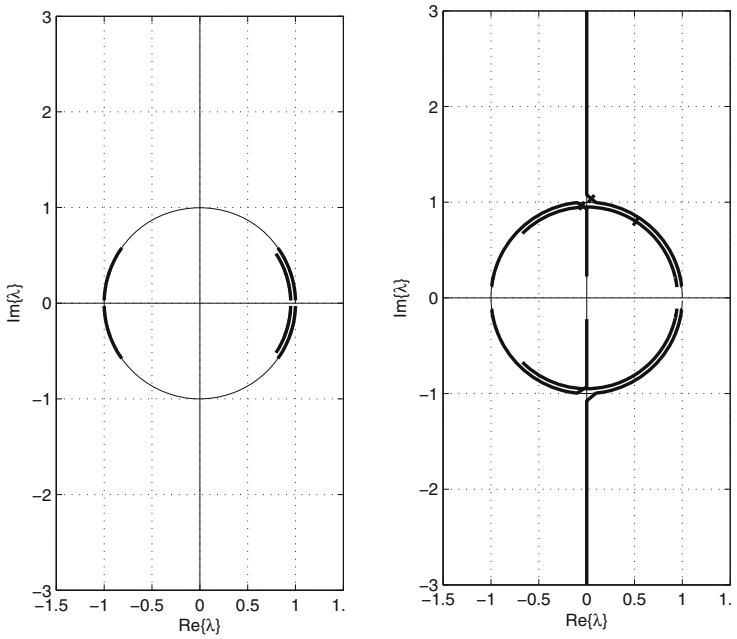

Fig. 7. Same as in Fig. 6 but for forward time-averaging (roots of Eq. (84)). In the left panel $\varepsilon^{1/2}\omega_s \Delta t_i < 1$ for all ε in the chosen range. For larger Δt_i (right panel) $\varepsilon^{1/2}\omega_s \Delta t_i$ can be smaller and greater than unity ($\lambda_{1,3} = (0, i)$ and $\lambda_{2,4} = (0, -i)$ if $\varepsilon^{1/2}\omega_s \Delta t_i = 1$).

Consider now the effect of the Asselin filter for the centered and forward time-averaging. Fig. 8 gives the result of calculation of eigenvalues of matrix M_c for $\alpha = 0.1$ (notice that by default POM uses $\alpha = 0.05$). It is helpful to compare this figure with Fig. 6. We see that the Asselin filter shifts the computational eigenvalues in the interior of the unit circle $|\lambda| = 1$ and almost does not modify the physical λ. This is due to the substantial difference in the periods of computational and physical

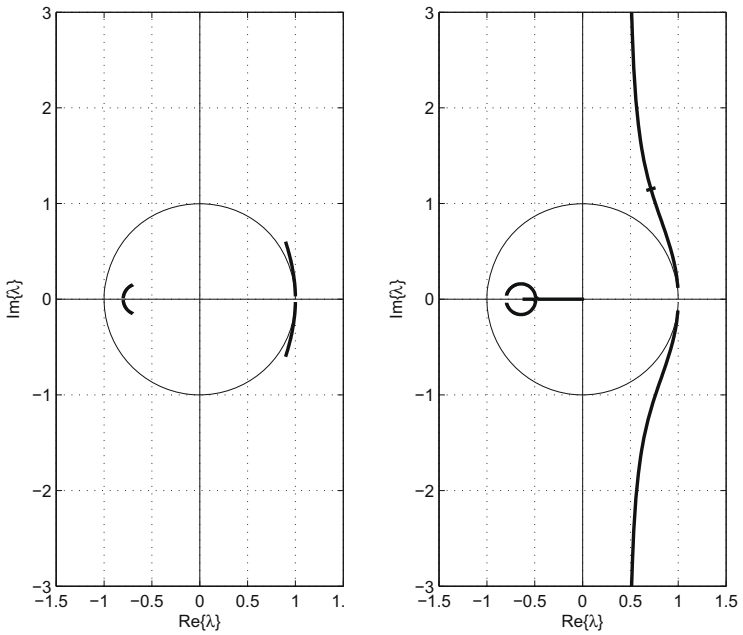

Fig. 8. The layout of eigenvalues λ of matrix M_c (centered time-averaging) with the Asselin filter for $\alpha = 0.1$ and $\omega_f \Delta t_i = 0.8\pi$ (left panel) and $\omega_f \Delta t_i = 3.2\pi$ (right panel) for ε in the range $[1 \cdot 10^{-3}, 0.4]$. We put marks on some curves to divide portions, for which $\varepsilon^{1/2}\omega_s \Delta t_i$ is smaller or greater than unity.

modes for $\alpha = 0$. Let us take limit cases. If $arg(\lambda) \sim \pi$, the period is approximately equal to $2\Delta t_i$ and the Asselin filter reduces $|\lambda|$. If $arg(\lambda) \sim 0$, the period is large and the filter does not practically modify λ. Thus computational modes will decay with time while the physical modes will remain practically unchanged. Fig. 8 shows that the Asselin filter cannot improve the stability of the scheme with centered averaging.

A similar effect of the Asselin filter is observed in the calculation of eigenvalues in the case of forward time-averaging (Fig. 9). It is interesting that for increasing ε in the right panel, the physical mode first appears to be decaying and then becomes unstable. Thus the instability occurs for smaller values of $\varepsilon^{1/2}\omega_s \Delta t_i$ as compared to the case without the Asselin

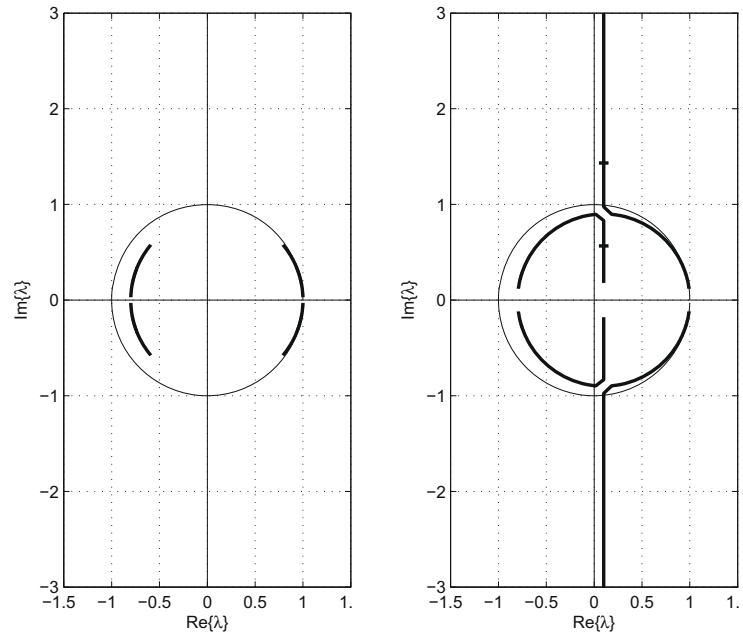

Fig. 9. The same as in Fig. 8 but for forward time-averaging.

filter. Strictly speaking, in this case we cannot recognize what modes became unstable – physical or computational ones (compare with the discussion of this feature in Fig. 7). Notice also a shift of eigenvalues to the right for not very small ε, as compared to the case of $\alpha = 0$ (Fig. 7).

The results of the outlined analysis will be compared with the corresponding results of the stability analysis of finite-difference schemes (28)–(36) and (28)–(34), (37), (38) in the following section.

9. Stability analysis of the POM time-splitting schemes

In this section we present the results of stability analysis of the POM time-splitting schemes with centered and forward time-averaging of the external mode variables. We will also consider the effect of the Asselin filter applied to both the external and internal variables of the model. Let us start with the case without the Asselin filter. For the stability analysis we introduce 8D-vector $\boldsymbol{\psi}^m$,

$$\boldsymbol{\psi}^m = \{u_a^{m,1}, \eta^{m,1}, u_a^{m-1,N}, \eta^{m-1,N}, u_1^{m+1}, \zeta^{m+1}, u_1^m, \zeta^m\}, \quad m = 1, 2, \ldots \tag{87}$$

and rewrite the finite-difference schemes (28)–(36) and (28)–(34), (37), (38) as

$$\boldsymbol{\psi}^{m+1} = M\boldsymbol{\psi}^m, \quad m = 1, 2, \ldots, \tag{88}$$

where 8×8 matrix M performs $2N$ external and one internal time steps integration of system (28)–(36) or (28)–(34), (37), (38). The matrix M depends on what type of time-averaging has been chosen. It will be different for schemes (28)–(36) and (28)–(34), (37), (38). In the case of the scheme with the Asselin filter, the matrix M takes into account some additional relations introduced by the Asselin filter (e.g. (77)), and the vector $\boldsymbol{\psi}^m$ is also modified in a way similar to (80).

For the stability analysis of the finite-difference scheme we calculate eigenvalues of the matrices M. Suppose that $\varepsilon = 0$. The eigenvalues of matrices M in this case are (see (D.7) and (D.8))

$$\lambda_{1,2} = \left[i\omega_f \Delta t_e \pm \sqrt{1 - (\omega_f \Delta t_e)^2}\right]^N; \quad \lambda_{3,4} = \left[-i\omega_f \Delta t_e \pm \sqrt{1 - (\omega_f \Delta_e)^2}\right]^N, \tag{89}$$

$$\lambda_5 = \lambda_7 = 1; \quad \lambda_6 = \lambda_8 = -1, \tag{90}$$

where the superscript N in (89) means raising to the power of N. We are interested in the scheme behavior for the $\omega_f \Delta t_e \leqslant 1$. Fig. 10 shows the layout of the eigenvalues (89), (90) on the corresponding complex plane. The pair of eigenvalues λ_2 and λ_4 describes the evolution of fast physical modes (hereafter denoted as FPM). The leap-frog time integration of the external mode equations produces fast computational modes (FCM) with λ_1 and λ_3. For $N = 1$ FCM eigenvalues have a phase shift of π with respect to FPM, which remains true for all odd N (λ_2 relative to λ_3 and λ_4 relative to λ_1). For even N FCM eigenvalues coincide with FPM eigenvalues. The eigenvalues λ_5 and λ_7 correspond to the slow physical modes (SPM), which have zero frequency for $\varepsilon = 0$. The eigenvalues λ_6 and λ_8 represent slow computational modes (SCM).

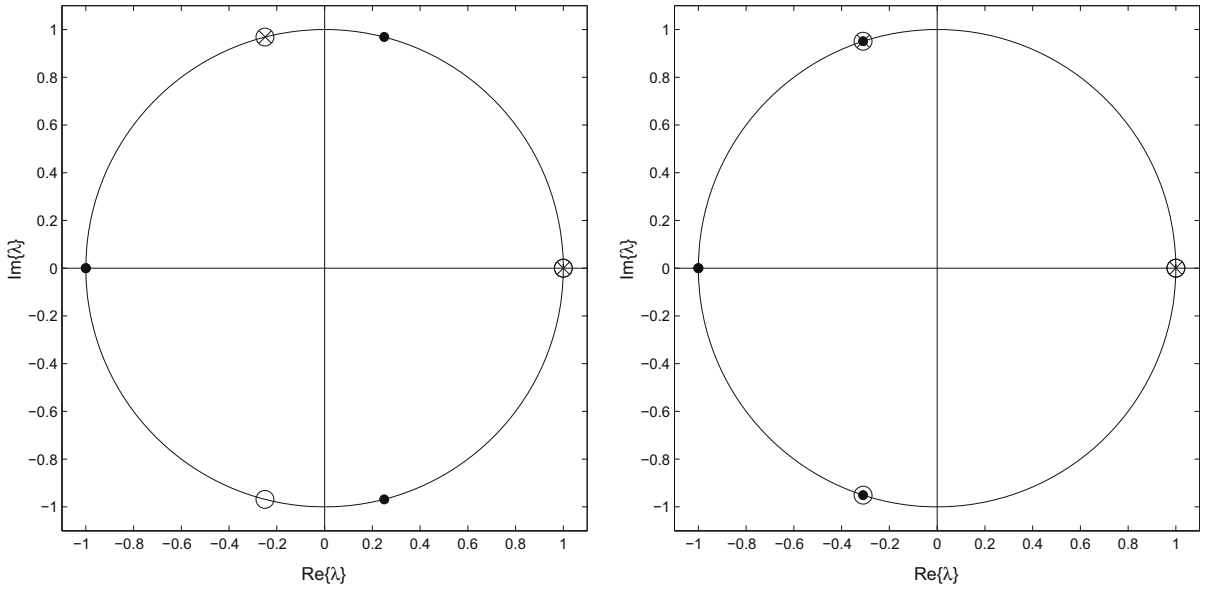

Fig. 10. The eigenvalues of the matrix M for $\varepsilon = 0, \omega_f \Delta t_e = 0.02\pi$, and $\Delta t_i = N\Delta t_e$, where $N = 29$ for the left panel and $N = 30$ for the right panel. Eigenvalues $\lambda_2, \lambda_4, \lambda_5, \lambda_7$ corresponding to the physical modes are denoted by circles. Eigenvalues $\lambda_1, \lambda_3, \lambda_6, \lambda_8$ corresponding to the computational modes are marked by dots. Additionally, values $\exp(i\omega_1 \Delta t_i)$ and $\exp(i\omega_2 \Delta t_i)$ are shown by crosses.

In the case of non-zero ε we calculate matrices M and solve corresponding eigenvalue problems numerically. First, we compute the elements of matrix M for a given set of parameters of the numerical scheme. Let $\{\mathbf{e}_l\}, l = 1,\ldots,8$ be an orthonormal basis in the 8D Euclidean linear space of vectors $\boldsymbol{\psi}$. We conduct one internal time step integration of the corresponding numerical scheme to find the vectors $\boldsymbol{\psi}_l, l = 1,\ldots,8$ resulting from the evolution of the basis vectors $\{\mathbf{e}_l\},\ l = 1,\ldots,8 : \psi_l = M\mathbf{e}_l, l = 1,\ldots,8$. The matrix elements $M_{k,l}$ are computed as projections of ψ_l onto the basis vectors $\mathbf{e}_k, k = 1,\ldots,8 : M_{k,l} = (\mathbf{e}_k, \boldsymbol{\psi}_l)$. The calculation of eigenvalues of matrix M is then performed with standard LAPACK routines [1].

Identification of the obtained eigenvalues as FPM, FCM, SPM and SCM eigenvalues is done as follows. We start computations with $\varepsilon_0 = 0$ and sort computed eigenvalues according to expressions (89) and (90). Then eigenvalues are calculated for $\varepsilon_1 = \varepsilon_0 + \delta\varepsilon$, with a sufficiently small increment $\delta\varepsilon$. To identify eigenvalues obtained for ε_1 we assume a continuous dependence of these eigenvalues on ε and sort eigenvalues according to the distance to the eigenvalues computed for ε_0, and so on.

Let us first discuss the stability of the conventional POM time-splitting scheme with centered time-averaging. In what follows, we consider examples of the scheme stability analysis for two magnitudes of $\omega_f\Delta t_e$: $\omega_f\Delta t_e = 0.02\pi$ (high time resolution of the external mode, 100 grid points per the period $T_f = 2\pi/\omega_f$) and $\omega_f\Delta t_e = 0.2\pi$ (low time resolution of the external mode, 10 grid points per the period T_f). Fig. 11 presents the results of eigenvalue computations for the case of high time resolution of the external mode. We consider the scheme properties for different $N = \Delta t_i/\Delta t_e$. For $\omega_f\Delta t_i \gg 1$ (sufficiently large N, right panels in Fig. 11) computed SPM and SCM eigenvalues should agree with the corresponding eigenvalues examined in Section 8 (Figs. 6 and 8). In the case of $\omega_f\Delta t_i \sim 1$ (smaller N, left panels in Fig. 11) one could expect different results for differential-difference and finite-difference analyses of SCMs and SPMs.

For $\omega_f\Delta t_i = 3.18\pi$ (Fig. 11, upper right panel) the results of analysis of differential-difference and finite-difference schemes practically coincide (compare right panels in the Figs. 6, 8, and 11). Without the Asselin filter (upper right panel in Fig. 11, right panel in Fig. 6) SPMs are unstable for all $\varepsilon > 0$, one of the SCMs is damped, another changes sign at every internal time step. The behavior of SPM and SCM eigenvalues as functions of ε is identical to the results of Section 8 even for large ε.

For $\omega_f\Delta t_i = 0.78\pi$ one SCM is unstable probably because of incomplete averaging of the fast modes in the finite-difference scheme (Fig. 11, upper left panel). Interestingly, unstable SCM does not change the behavior of SPM: instability rates found by the analyses of differential-difference and the finite-difference schemes agree well.

FPMs of the POM time-splitting scheme (Fig. 11, upper panels) appear to be marginally unstable for the whole range of ε. Note that despite the high temporal resolution of the external mode, FPMs do not reproduce frequency variation $\omega_1(\varepsilon)$ of the analytical solution. In the left panels of Fig. 11 the frequency of FPMs for large ε remains close to ω_f. In the right panels of Fig. 11 frequencies of FPM differ from the analytical solution even for small ε. These conclusions agree with the result of asymptotic analysis (Section 6); namely that the fast component of u_a, η are reproduced correctly on rather small time interval (on the order of the slow mode period). As can be seen in the upper panels of Fig. 11, FCM eigenvalues can be very close to eigenvalues of SPM. FCMs are neutrally stable and the corresponding frequencies appear to be independent of ε.

The lower panels in Fig. 11 illustrate the effect of the Asselin filter on eigenvalues of the matrix M for the same set of parameters of the numerical scheme. The Asselin filter efficiently damps FCM and SCM but does not improve stability of physical modes. FCM modes are completely filtered out ($|\lambda| \ll 1$) because of the high time resolution of the external mode and the large number of N. SCMs are stable for the range of ε examined in Fig. 11. Simultaneously SPMs remain unstable with instability rates practically unaffected by filtering. A comparison of Figs. 8 and 11 confirms that the differential-difference stability analysis correctly predicts properties of SCMs and SPMs of the POM scheme with the Asselin filter for the case $\omega_f\Delta t_i \gg 1$ (right panel of Fig. 8 and right lower panel in Fig. 11) and even for $\omega_f\Delta t_i \sim 1$ (left lower panel in Fig. 11).

Fig. 12 presents an example of the eigenvalue calculation for the case of low time resolution of the external mode ($\omega_f\Delta t_e \sim 1$). Stability properties of different modes remain similar to the case of high time resolution of the external mode (compare Figs. 12 and 11). Note only that FPMs do not have frequency ω_f for small ε and become marginally damped in the case of $\omega_f\Delta t_i \sim 1$ (Fig. 12, left upper panel). The instability rate of SPMs is not affected by the low time resolution in the case of small N (left upper panel). For larger even values of N (right upper panel) an increase in the instability rate for both SPM and FPM is noticeable, while the behavior of computational modes does not change with respect to the case of high time resolution of the external mode.

The lower panels in Fig. 12 illustrate the effect of the Asselin filter on eigenvalues of the matrix M for the same set of parameters of the numerical scheme. For small even values of N (Fig. 12, left lower panel) FPMs are attenuated much stronger as compared to the case of high time resolution (Fig. 11, left lower panel), and FCMs are not damped completely. The Asselin filter fails to enforce stability of SCMs for large ε. SPMs remain marginally unstable but the instability rates are clearly reduced compared to the results presented in the upper panels of Fig. 12. As expected, for larger N (Fig. 12, right lower panel) the layout of eigenvalues is more similar to the results presented in the right panel of Fig. 8 and right lower panel of Fig. 11. Note only that FPMs are strongly damped in the case of low time resolution, while the instability rate of the SPMs is not affected significantly by the Asselin filter. The phase errors of SPMs are acceptable at low ε in all plots of Fig. 12.

The case of $\omega_1\Delta t_e \sim 1$ and $\omega_2\Delta t_i \sim 1$ (Fig. 12, right panel) corresponds to the most common practical choice of the POM time-splitting scheme parameters. It appears that for this choice of parameters, properties of the POM time-splitting scheme are quite sensitive to N, which determines the time-averaging period of the external mode. Fig. 13 shows eigenvalues of the matrix M when N is augmented by 1 with respect to the case considered in Fig. 12. For odd N (Fig. 13, upper panels) the layout of eigenvalues of the matrix M differs substantially from layouts in the upper panels of Figs. 11 and 12. FPMs become the

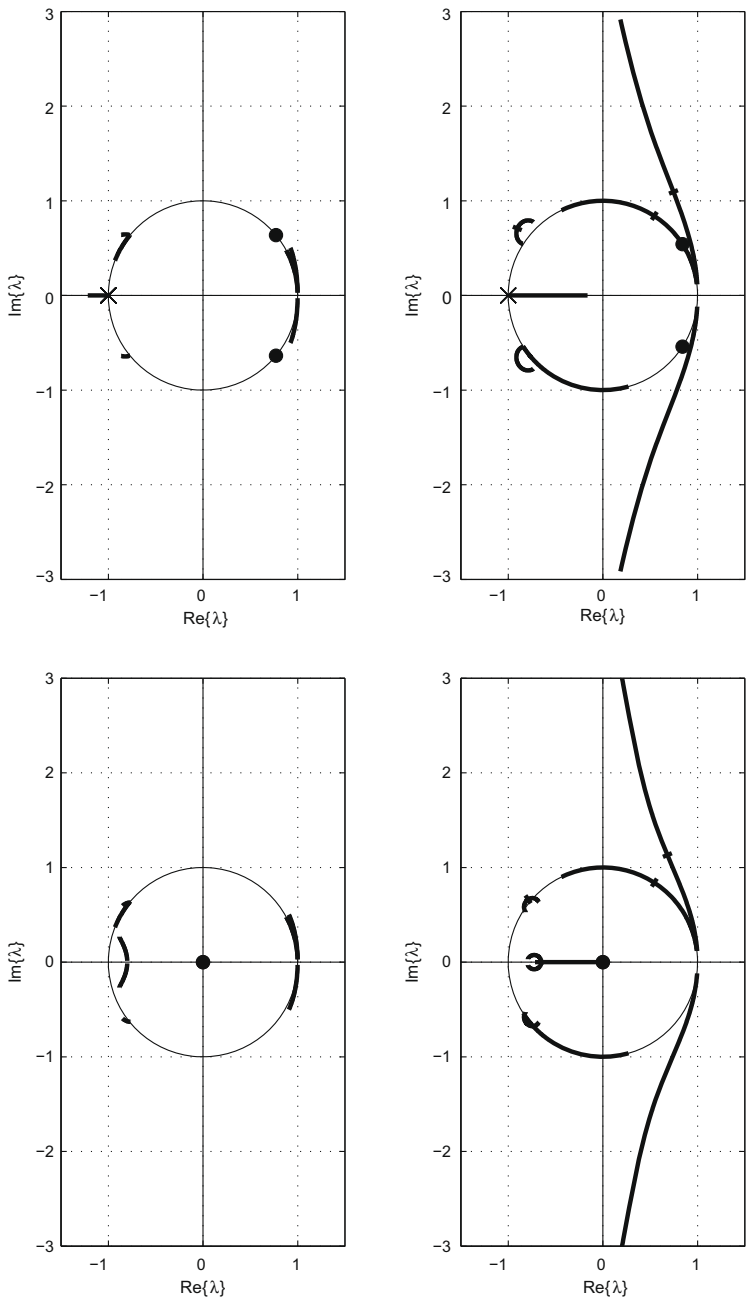

Fig. 11. The layout of eigenvalues of matrix M for the centered time- averaging scheme for ε in the range $[1 \cdot 10^{-3}, 0.4]$ and $\omega_f \Delta t_e = 0.02\pi$. For the left panels $N = 39$ and $\omega_f \Delta t_i = 0.78\pi$. For the right panels $N = 159$ and $\omega_f \Delta t_i = 3.18\pi$. In the upper panels no Asselin's filter is applied, for the lower panels the Asselin filter is used with $\alpha = 0.1$. FCM eigenvalues do not vary with ε and are shown with dots. In the upper panels SCM eigenvalue $\lambda = -1$, which do not change with ε, is shown by crosses. Variations of other eigenvalues with ε are shown with bold lines. Bold segments of the unit circle show $\exp(i\omega_1 \Delta t_i)$ and $\exp(i\omega_2 \Delta t_i)$ for the same range of ε. Note that on the left panels $0.78\pi \leqslant \omega_1 \Delta t_i < \pi$ while on the right panels $3.18\pi \leqslant \omega_1 \Delta t_i < 4\pi$. For reference we put marks on some curves to divide portions, for which $\varepsilon^{1/2} \omega_s \Delta t_i$ is smaller or greater than unity.

fastest growing unstable modes of the scheme, while SCMs become stable for small N. SPMs remain unstable for odd N, but strong instability of SPM at large ε in the upper right panels of Figs. 11 and 12 is replaced in Fig. 13 by the strong instability of FPM for values of ε larger than $5 \cdot 10^{-3}$.

For small odd N (Fig. 13, upper left panel) the Asselin filter does not result in a qualitative change in the properties of the POM time-splitting scheme, except for a significant attenuation of FCMs. Eigenvalues of the POM scheme with the Asselin filter for small odd values of N (Fig. 13, left lower panel) show a pattern which differs from the eigenvalue distribution for small even values of N (Fig. 12, left lower panel). An increment of N by 1 makes SCM eigenvalues stable and real for

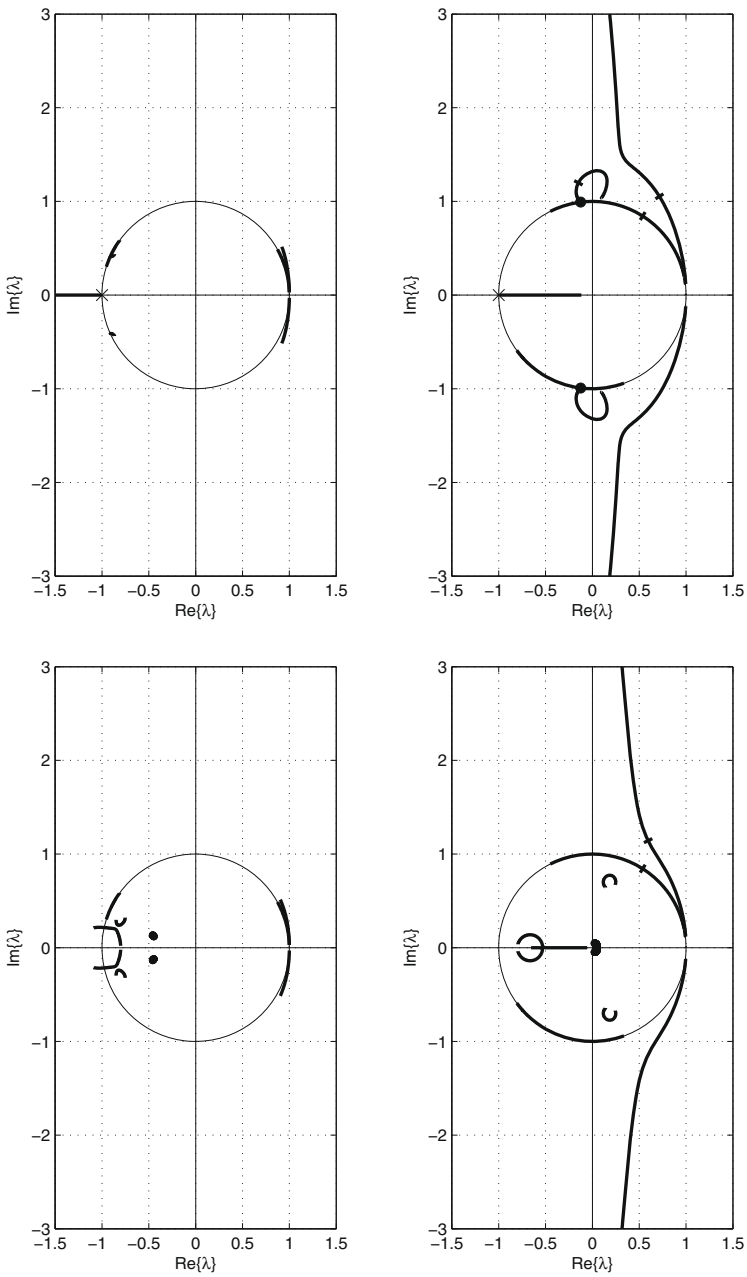

Fig. 12. Same as Fig. 11 but for $\omega_f \Delta t_e = 0.2\pi$. For the left panels $N = 4, \omega_f \Delta t_i = 0.8\pi$. For the right panels $N = 16, \omega_f \Delta t_i = 3.2\pi$. In the upper panels no Asselin's filter is applied, for the lower panels the Asselin filter is used with $\alpha = 0.1$. In the left upper panel FCM eigenvalues are not shown since they are close to FPM eigenvalues. In other panels FCM eigenvalues are shown with dots. In the upper panels, SCM eigenvalue $\lambda = -1$, which does not change with ε, is shown by crosses. Variations of other eigenvalues with ε are shown with bold lines. Bold segments of the unit circle show $\exp(i\omega_1 \Delta t_i)$ and $\exp(i\omega_2 \Delta t_i)$ for the same range of ε (compare with Fig. 11).

the whole range of ε. The stability of SPMs in Fig. 13 (left lower panel) is improved by the Asselin filter to a smaller extent as compared to the case of small even values of N (Fig. 12, left lower panel). FPMs are strongly unstable for large ε.

For larger odd values of N the application of the Asselin filter causes significant change of the eigenvalue layout (Fig. 13, right lower panel). The most unstable mode is SPM, while FPMs are strongly damped. On the other hand, the eigenvalue distribution is similar to the results presented in the right lower panels of Figs. 11 and 12, and in the right panel of Fig. 8. This confirms the applicability of the differential-difference stability analysis for sufficiently large $\omega_f \Delta t_i$. The major drawback of this POM time-splitting scheme is the instability of SPMs, which cannot be removed by the application of the Asselin filter with coefficients $\alpha \sim 0.1$ typically used in practice.

marize the analysis of the POM time-splitting scheme with centered time-averaging of the external mode vari-
resent the plots of the largest $|\lambda|$ as a function of $\omega_2\Delta t_i$ and ε (Fig. 14). The reduction of $|\lambda|$ for small $\omega_2\Delta t_i$ is mainly
reduction of Δt_i. For computational reasons we have chosen contours (bold) $|\lambda| = 1.01$ as the boundary of the sta-
n for the scheme. This boundary is approximate and actually to the left of it $|\lambda|$ is still greater than unity.
pper left panel the contour $|\lambda| = 1.01$ is not shown since it is very close to the ordinate axis and is quite irregular
merical noise in $|\lambda|$ calculations at small N).
n be seen in Fig. 14, the rate of instability depends on the ratio of the period of averaging of the external mode
the period of the fast mode T_f. Averaging over an integer number of the fast mode periods occurs when
$, n = 1, 2, 3, \ldots$ (the dashed lines in Fig. 14). Obviously the dependence on $\omega_f\Delta t_i$ is more pronounced when

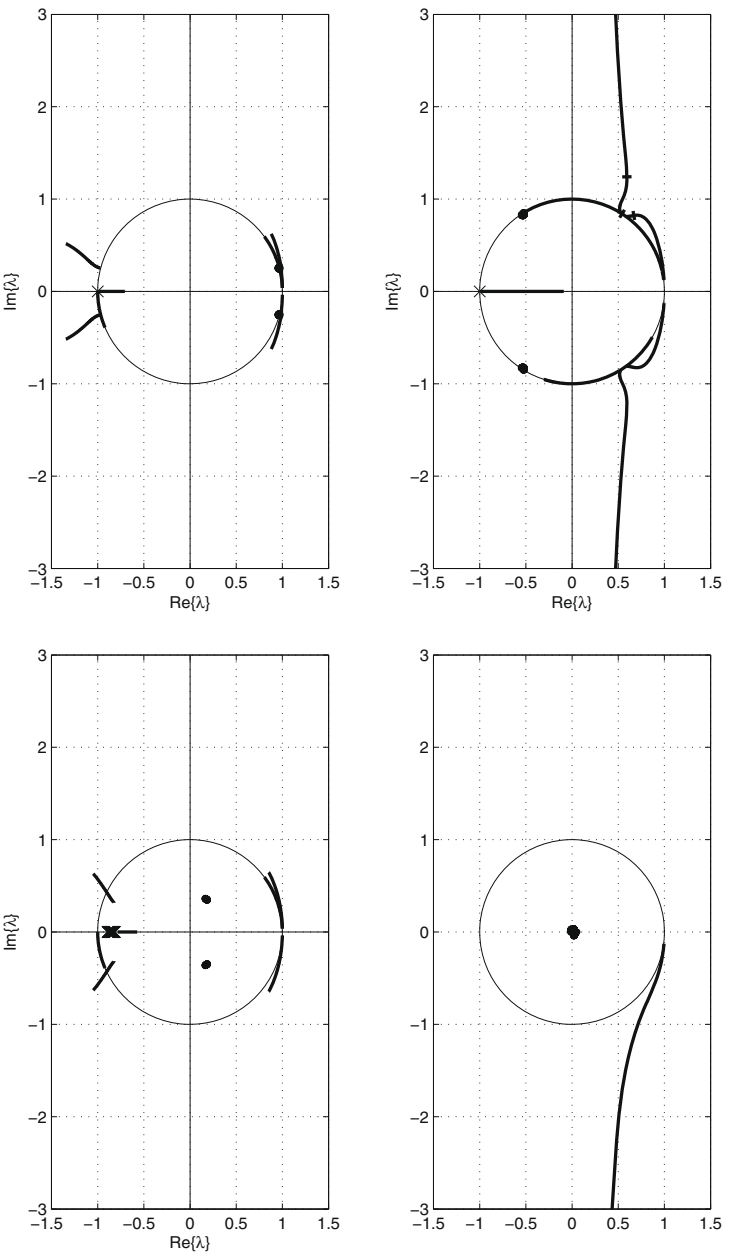

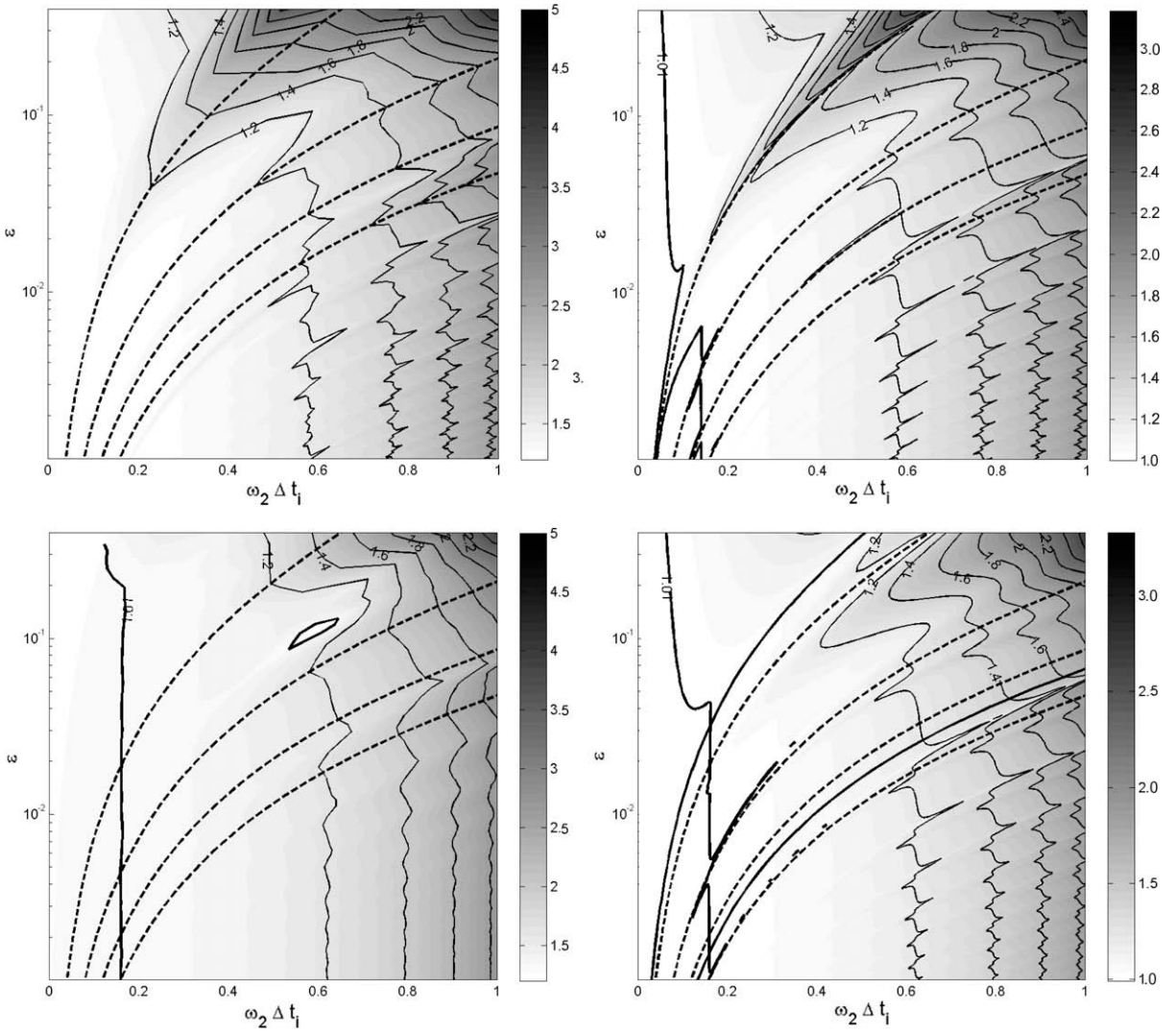

Fig. 14. The largest modulus of eigenvalues of the matrix M for the POM scheme with centered time-averaging as a function of $\omega_2\Delta t_i$ and ε. For the left panels $\omega_f\Delta t_e = 0.2\pi$. For the right panels $\omega_f\Delta t_e = 0.02\pi$. The upper panels represent the results without the Asselin filter, while the lower panels represent the results with the Asselin filter, $\alpha = 0.1$. Bold contours ($|\lambda| = 1.01$) approximate the boundary of the stability region (not shown in the upper left panel). Dashed lines are the contours of constant $\omega_f\Delta t_i = n\pi$, where $n = 1$ (the uppermost curve), 2, 3 and 4. Additionally, in the lower right panel, the contours of constant $\omega_f\Delta t_i = 0.8\pi$ and $\omega_f\Delta t_i = 3.2\pi$ are shown with bold lines.

$\Delta t_i \sim T_f$. In the left upper panel the $\omega_f\Delta t_i = \pi$ corresponds to a narrow and steep trough in the $|\lambda|$ distribution located between two pronounced ridges with high instability rates. For longer integration times of the external mode (and for the low time resolution of the external mode) the lines of $\omega_f\Delta t_i = n\pi$ do not coincide with the troughs of $|\lambda|$ due to the phase errors of the scheme, however troughs and ridges in $|\lambda|$ distribution are clearly seen and are parallel to lines of $\omega_f\Delta t_i = const$. The examples of eigenvalue computations presented in Figs. 11 and 12 are produced for $\omega_f\Delta t_i = 0.8\pi$ and $\omega_f\Delta t_i = 3.2\pi$. The corresponding curves of constant $\omega_f\Delta t_i$ are shown with bold lines in the lower right panel of Fig. 14. The line $\omega_f\Delta t_i = 0.8\pi$ is located on the slope of the first ridge of $|\lambda|$ distribution for all experiments, while the case of $\omega_f\Delta t_i = 3.2\pi$ corresponds to the set of "non-resonant" parameters of the scheme which are neither on the ridge nor in the trough of $|\lambda|$.

Fig. 14 supports the result of our analysis discussed in Section 8 that the POM time-splitting scheme is unconditionally unstable for all ε. The Asselin filter does not improve the stability of the scheme at least at small ε (e.g. compare location of the bold contours in the right panels of Fig. 14) because for this scheme the most unstable modes are SPMs. Notice that in general the instability rate grows faster than linearly with increasing $\omega_2\Delta t_i$. That is why the common practical recommendation for the choice of Δt_i on the verge of the stability requirement ($\omega_2\Delta t_i \sim 1$) seems to be questionable (see modulus isolines on Fig. 14 for $\omega_2\Delta t_i \sim 1$). Our analysis indicates that practically acceptable instability rates for the POM time-splitting scheme with centered time-averaging are observed if $\omega_f\Delta t_i \gg 1$ and $\omega_2\Delta t_i \ll 1$.

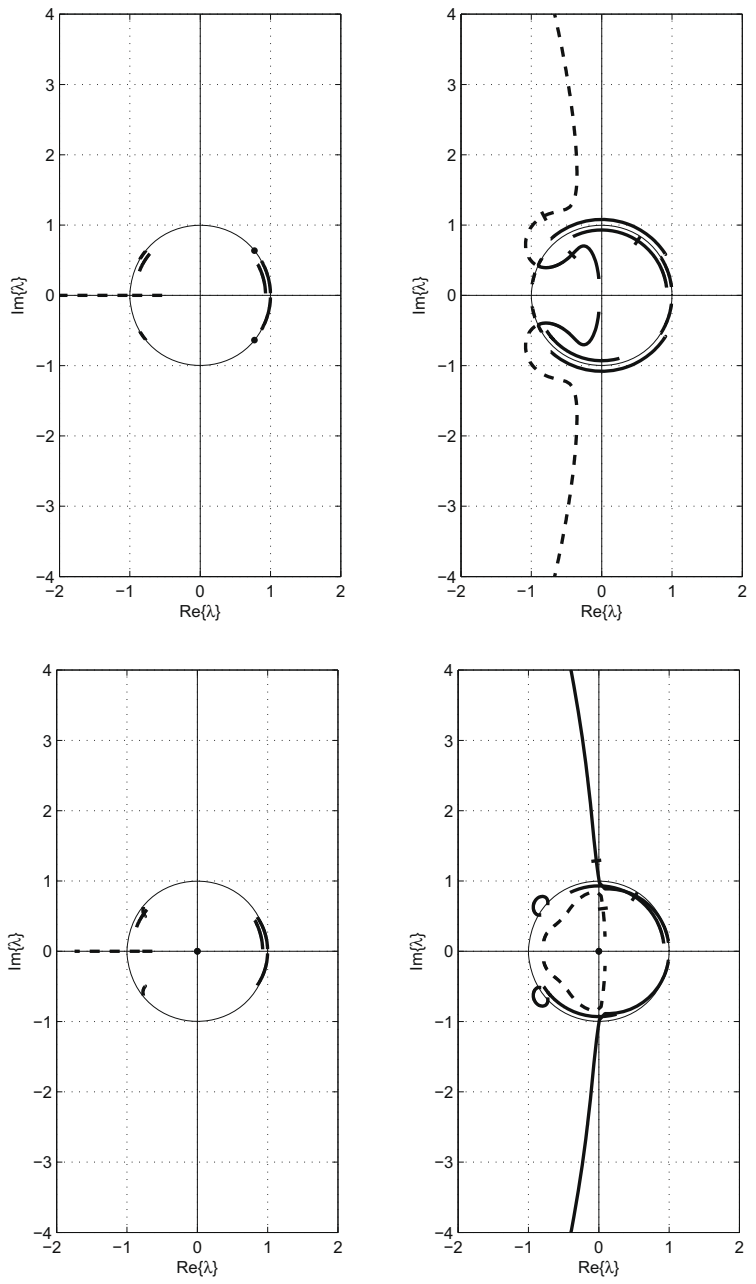

Fig. 15. The layout of eigenvalues of matrix M for the forward time-averaging scheme for ε in the range $(10^{-3}; 0.4)$. For these plots $\omega_f \Delta t_e = 0.02\pi$. Left panels: $N = 39, \omega_f \Delta t_i = 0.78\pi$, right panels: $N = 159, \Delta t_i \omega_f = 3.18\pi$. Upper panels represent the results without the Asselin filter, lower panels with the Asselin filter, $\alpha = 0.1$. SCM eigenvalues are shown with dashed lines. In the lower panels and in the upper left panel FCM are shown by dots. In the right upper panel FCM eigenvalues are scaled by a factor of 1.05. Variations of other eigenvalues with ε are shown with bold lines. The bold curves representing $\exp(i\omega_1 \Delta t_i)$ and $\exp(i\omega_2 \Delta t_i)$ are scaled by 0.95 in all panels. For reference we put marks on some curves to divide portions for which $\varepsilon^{1/2}\omega_s \Delta t_i$ is smaller or greater than unity.

The stability analysis of the differential-difference scheme conducted in Section 8 shows that a straightforward modification of the POM time-splitting scheme, namely, the application of forward time-averaging (see (66), (67) and (72)) of the external mode variables, results in the conditionally stable scheme. In fact, under the assumptions that $\omega_f \Delta t_e \ll 1$ (high resolution of the external mode), $\omega_f \Delta t_i \gg 1$ (averaging of the external mode over many periods T_f) and small values of ε the scheme is stable, if $\varepsilon^{1/2}\omega_s \Delta t_i < 1$. It has non-growing SCMs, and reproduces SPMs with minimal amplitude and phase errors (see Fig. 7). Let us consider properties of the time-splitting scheme with forward time-averaging for a more practical choice of Δt_e and Δt_i.

Fig. 15 presents the eigenvalues of the matrix M in the case of $\omega_f \Delta t_e \ll 1$ (high time resolution of the external mode). For $\omega_f \Delta t_i = 0.78\pi$ (left upper panel) the only unstable modes are SCMs. This instability is not predicted by differential-difference analysis since $\omega_f \Delta t_i \sim 1$ for the considered case. All other eigenvalues are located on the unit circle and are neutrally stable for the whole range of ε variation. Notice also that the phase errors for SPMs are very small. FCM eigenvalues show no dependence on ε in this case.

For better time-averaging with $\omega_f \Delta t_i = 3.18\pi$ (Fig. 15, right upper panel) there exists a range of ε for which all modes are stable. SCMs become unstable at $\varepsilon > 4.5 \cdot 10^{-3}$, simultaneously FPMs become attenuated. At the threshold value of $\varepsilon = 4.5 \cdot 10^{-3}$, SCM and FPM eigenvalues become equal and, strictly speaking, we cannot identify which of these modes be-

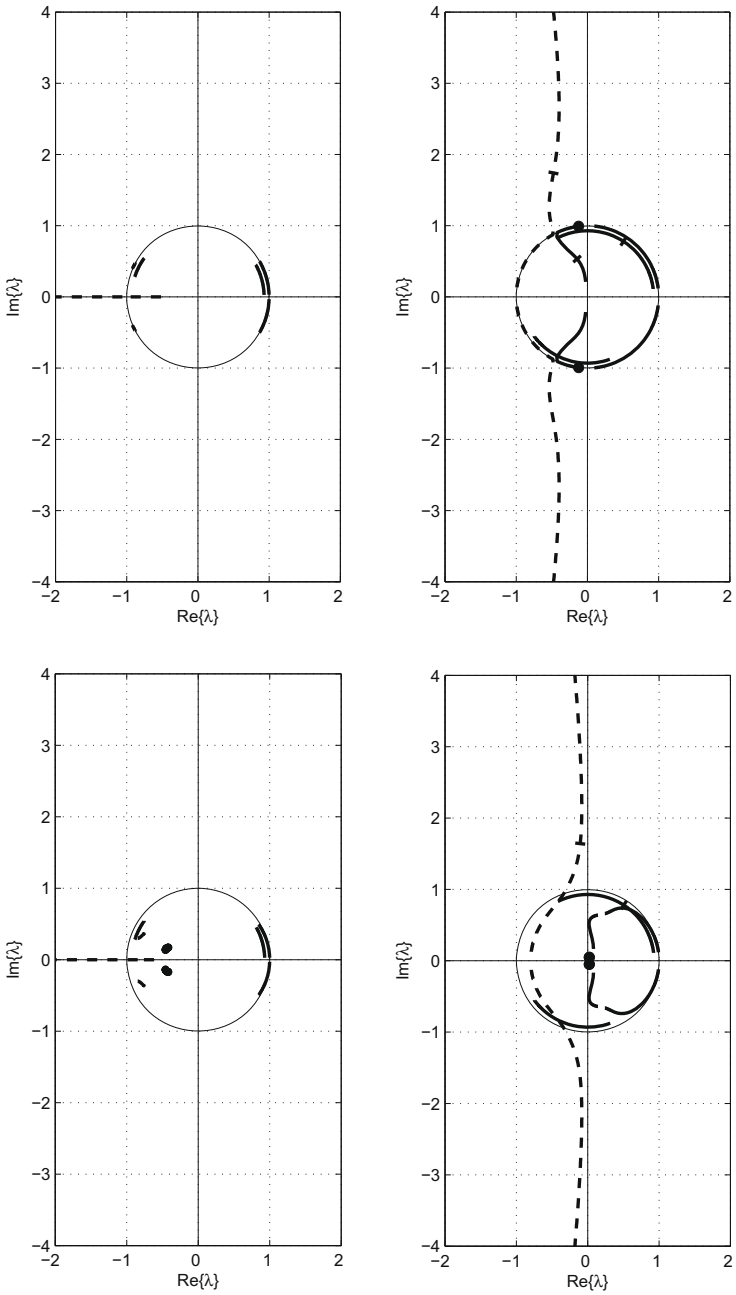

Fig. 16. Same as Fig. 15 but for $\omega_f \Delta t_e = 0.2\pi$. Left panels: $N = 4, \omega_f \Delta t_i = 0.8\pi$; right panels: $N = 16, \omega_f \Delta t_i = 3.2\pi$. Upper panels represent the results without the Asselin filter, lower panels with the Asselin filter, $\alpha = 0.1$. SCM eigenvalues are shown with dashed lines. FCM eigenvalues are close to FPMs and are not shown in the left upper panel. In lower panels and in the upper right panel FCM eigenvalues are shown by dots. Variations of other eigenvalues with ε are shown with bold lines. The bold curves representing $\exp(i\omega_1 \Delta t_i)$ and $\exp(i\omega_2 \Delta t_i)$ are scaled by 0.95.

comes unstable. In the vicinity of the threshold value of ε both SPMs and FPMs have large phase errors. Note also that FCMs exhibit significant dependence on ε and have frequencies which are close to frequencies of SPMs. Consequently, computational and physical modes are difficult to separate in the solution of the numerical scheme without the Asselin filter.

In the case of $\omega_f \Delta t_i = 0.78\pi$ (Fig. 15, left lower panel) the Asselin filter with $\alpha = 0.1$ removes completely FCMs ($|\lambda| \ll 1$) but fails to improve stability of SCMs, which undermines the practical utilization of this scheme for $\omega_f \Delta t_i \sim 1$. For larger $\omega_f \Delta t_i$ (Fig. 15, right lower panel) the Asselin filter damps SCMs and FCMs effectively, but at the expense of marginal instability of FPMs. Interestingly, the Asselin filter reduces phase errors of SPMs in the range of ε where these modes are stable. At the threshold value of $\varepsilon \sim 1 \cdot 10^{-2}$ SCM and SPM eigenvalues become equal and for larger ε one of these modes becomes

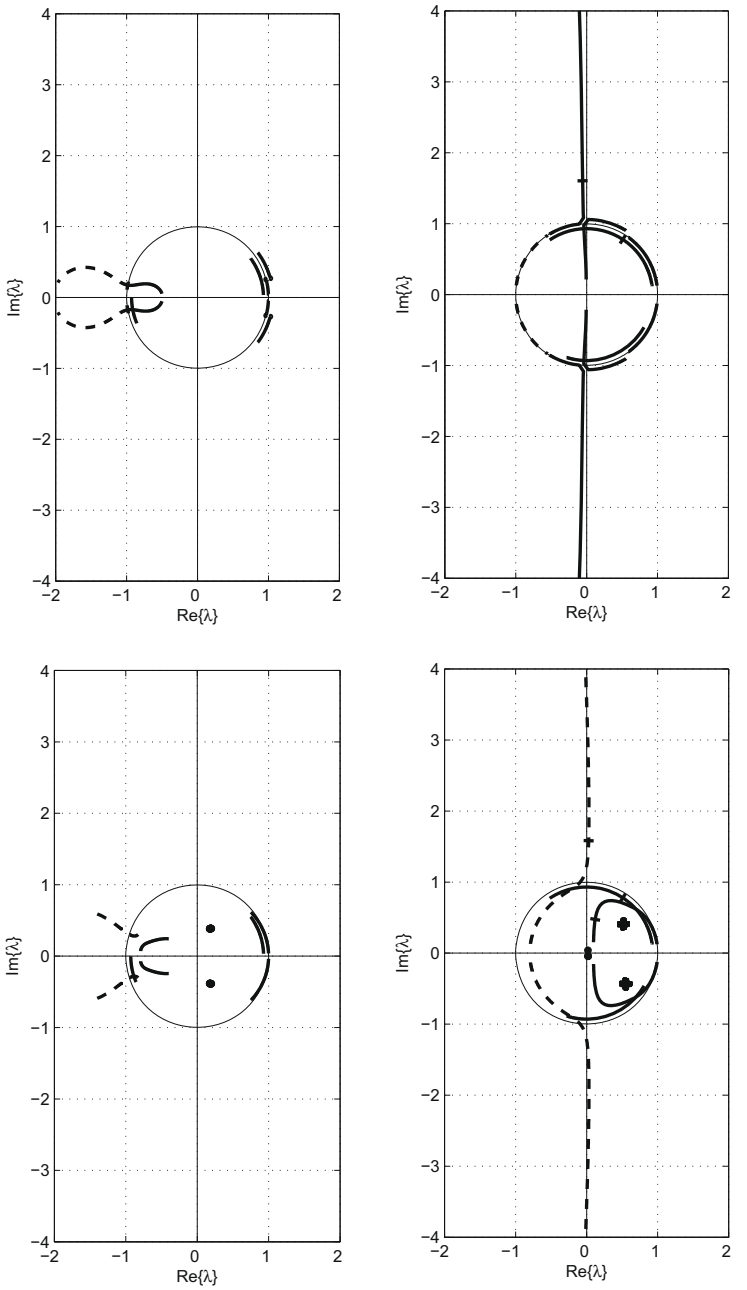

Fig. 17. Same as Fig. 16 but for $N = 5$ and $N = 17$. For all panels $\omega_f \Delta t_e = 0.2\pi$. For the left panels $\omega_f \Delta t_i = \pi$, for the right panels $\omega_f \Delta t_i = 3.4\pi$. Upper panels represent the results without the Asselin filter, lower panels with the Asselin filter, $\alpha = 0.1$. SCM eigenvalues are shown with dashed lines. In the lower panels FCM eigenvalues are shown by dots. The plus signs in the right lower panel show locations of the FPM eigenvalues. Variations of other eigenvalues with ε are shown with bold lines. For upper panels FCM eigenvalues are scaled by 1.05. The bold curves representing $\exp(i\omega_1 \Delta t_i)$ and $\exp(i\omega_2 \Delta t_i)$ are scaled by 0.95 in all panels.

strongly unstable. Nevertheless, for sufficiently small ε and for the set of parameters used in the right panels of Fig. 15 the scheme with forward time-averaging has clearly better stability properties than the conventional POM time-splitting scheme with centered time-averaging.

For lower time resolution of the external mode ($\omega_f \Delta t_e \sim 1$) and even values of N the behavior of the scheme remains similar to the high time resolution case (Fig. 16). In the case of $\omega_f \Delta t_i = 0.78\pi$ (left upper panel) the only unstable mode is one of SCMs. All other eigenvalues are neutrally stable for the whole range of ε variation. Phase errors for SPMs are very small. The major drawback of the scheme for this set of parameters is the instability of SCM which cannot be removed by the Asselin filter with $\alpha = 0.1$ (Fig. 16, left lower panel).

In the case of $\omega_f \Delta t_i = 3.2\pi$ (Fig. 16, right upper panel) the threshold value of ε is increased to $3.3 \cdot 10^{-2}$. If $\varepsilon < 3.3 \cdot 10^{-2}$ all modes are stable. At the threshold value of ε, SCM and FPM eigenvalues become equal. For $\varepsilon > 3.3 \cdot 10^{-2}$ FPMs are strongly attenuated and SCMs are strongly unstable. The Asselin filter damps FCMs effectively (Fig. 16, right lower panel) but does not change substantially the threshold value of ε. SCMs become unstable at approximately $\varepsilon = 3 \cdot 10^{-2}$, simultaneously SPMs are attenuated. FPMs are strongly damped by the Asselin filter especially for large ε.

As in experiments with the conventional POM scheme, the properties of the time-splitting scheme with forward time-averaging are sensitive to N, which determines the time-averaging period of the external mode. Layout of the eigenvalues

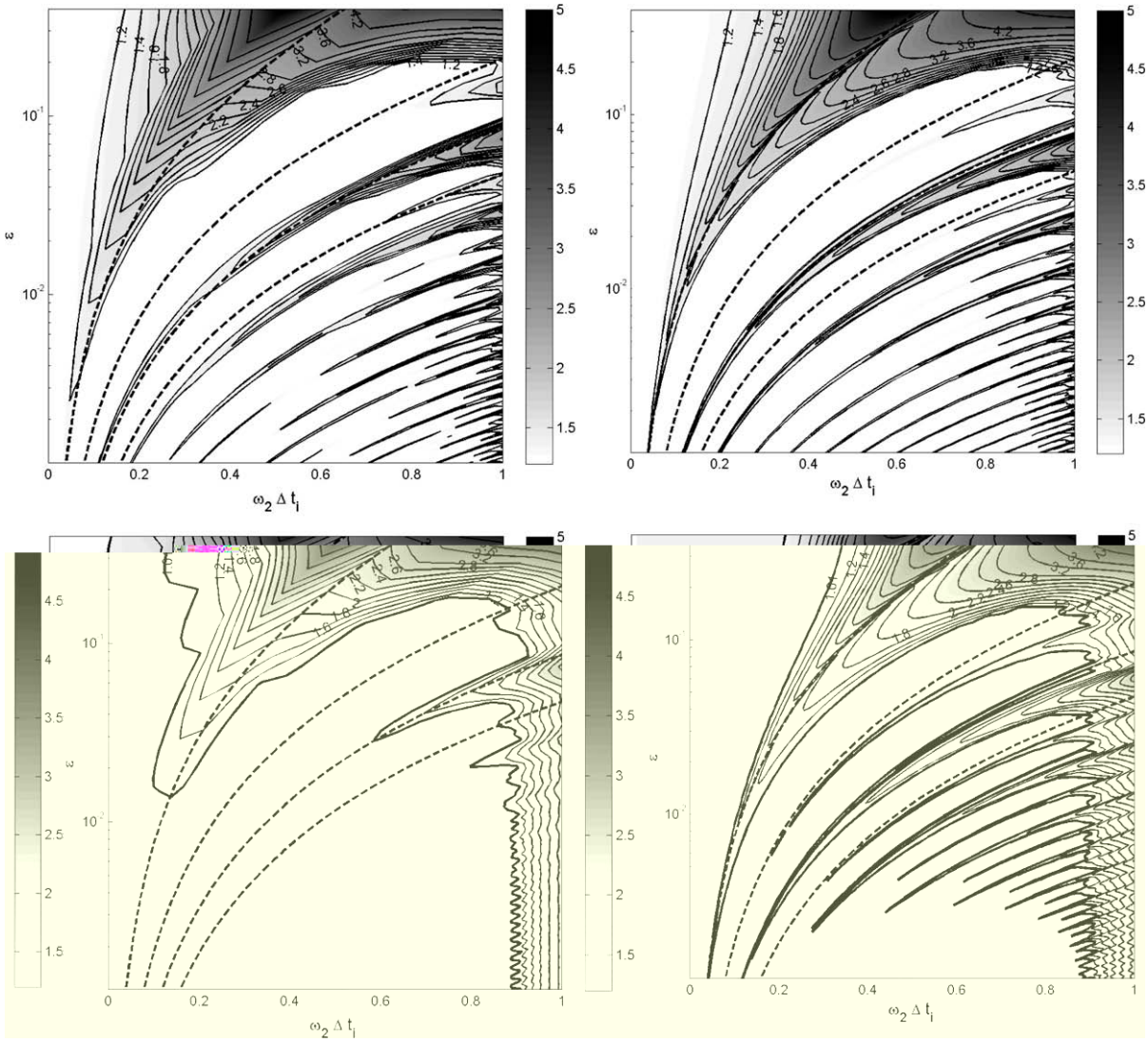

Fig. 18. The largest modulus of eigenvalues of the matrix M for the scheme with forward time-averaging as a function of $\omega_2 \Delta t_i$ and ε. For the left panels $\omega_f \Delta t_e = 0.2\pi$. For the right panels $\omega_f \Delta t_e = 0.02\pi$. The upper panels represent the results without the Asselin filter, while the lower panels represent the results with the Asselin filter, $\alpha = 0.1$. Bold contours ($|\lambda| = 1.01$) approximate the boundary of the stability region (not shown in the upper panels). Dashed lines are the contours of constant $\omega_f \Delta t_i = n\pi$, where $n = 1$ (the uppermost curve), 2, 3 and 4.

for N augmented by 1 with respect to the experiments presented in Fig. 16 shows some important differences (Fig. 17). For $N = 5$ (Fig. 17, upper left panel) the only unstable mode is SCM, which has complex conjugate eigenvalues in this case. In contrast to Fig. 16 upper left panel, the scheme is neutrally stable for ε in the range $[1 \cdot 10^{-3}, 1.6 \cdot 10^{-3}]$. For ε equal to the threshold value eigenvalues of SCM and FPM become equal. For ε greater than the threshold value FPMs are damped, while SCMs become unstable. SPMs and FCMs are neutrally stable for the whole range of ε. SPMs show significant phase errors at large ε. FCMs exhibit strong dependence on ε and have frequencies which are close to frequencies of SPMs. The Asselin filter significantly damps fast modes of the scheme for $N = 5$, but is unable to prevent instability of SCMs (Fig. 17, lower left panel). The range of parameters, for which the scheme is stable, remains approximately unchanged. Interestingly, the phase errors of the SPMs are substantially reduced by the Asselin filter without introduction of visible damping of these modes.

For $N = 17$, all modes are neutrally stable for $\varepsilon = [1 \cdot 10^{-3}, 5.0 \cdot 10^{-2}]$. For ε equal to the threshold value eigenvalues of FCM and FPM are equal and for larger ε one of these fast modes becomes strongly unstable, while the other is attenuated. Both SPM and SCM are neutrally stable for the whole range of ε. For $N = 17$, as in the case with $N = 5$, SPMs have significant phase errors at large ε. FCMs exhibit strong dependence on ε and have frequencies which are close to frequencies of SPMs. The Asselin filter changes the fastest growing mode of the scheme (Fig. 17, right lower panel). Fast modes are strongly attenuated with FCMs having $|\lambda| \ll 1$. For ε greater than the threshold value (which is not modified by the Asselin filter), SCMs become strongly unstable, while SPMs are damped. Within the stability range of ε phase errors of SPMs are reduced by the Asselin filter.

Finally we present the plots of the largest $|\lambda|$ as a function of $\omega_2 \Delta t_i$ and ε for the forward time-averaging scheme (Fig. 18). Unlike in Fig. 14 for the conventional scheme with centered time-averaging, we see some stability regions in Fig. 18. Bold contours $|\lambda| = 1.01$ shown in the lower panels of Fig. 18 represent a reasonable approximation to the boundary of the stability region for the scheme. These bold contours are close to the contour $|\lambda| = 1.2$ (especially for the case $\omega_f \Delta t_e = 0.02\pi$, right lower panel) indicating a fast drop of $|\lambda|$ to $|\lambda| = 1$. Contours $|\lambda| = 1.01$ are not shown in the upper panels of Fig. 18, because these bold lines shade the fine structure of contours of $|\lambda|$ for large $\omega_2 \Delta t_i$.

Fig. 18 supports results of Section 8 that the scheme with forward time-averaging is conditionally stable for $\omega_f \Delta t_e \ll 1$ (high temporal resolution of the external mode), $\omega_f \Delta t_i \gg 1$ (time-averaging of the external mode over many periods T_f), and $\omega_2 \Delta t_i < 1$. Moreover, as it can be seen in the lower left panel of Fig. 18, the forward time-averaging scheme has extended continuous region of stability for the case of low temporal resolution of the external mode, if the unstable computational modes are damped by the Asselin filter. The other panels of Fig. 18 show that except for the resonant ridges, the discussed scheme is stable for wide range of ε and $\omega_2 \Delta t_i$ including the regions with $\omega_f \Delta t_i \sim 1$ and $\omega_f \Delta t_i \gg 1$. On the other hand, outside of the stability region of the parameters, the instability in the scheme with forward time-averaging develops approximately two times faster than in the conventional POM time-splitting scheme. The rate of instability is more sensitive to the ratio of the averaging period of the external mode (Δt_i) to the period of the fast mode (T_f), as can be seen in Fig. 18 by the resonance structure having pronounced ridges and troughs. It is interesting that despite the fact that the time-averaging period in the considered scheme is half that of the scheme with centered time-averaging, the dashed line $\omega_f \Delta t_i = \pi$ (half period averaging) coincides with the first steep trough in the distribution of the $|\lambda|$ in the right upper panel of Fig. 18. For the case of high temporal resolution of the external mode, the Asselin filter reduces the rates of instability of the scheme but is not able to suppress resonant instability ridges and extend considerably the stability region of parameters.

In all presented examples of eigenvalue layouts the POM time-splitting scheme with forward time-averaging reproduces amplitudes and phases of SPMs with smaller errors compared to the conventional POM time-splitting scheme with centered time-averaging. Moreover, SPMs are always stable. FPMs are also always stable, but the phase errors are small only if the fast mode period is well resolved ($\omega_f \Delta t_e \ll 1$). For a practically important set of parameters: $\omega_f \Delta t_e \sim 1$, $\omega_f \Delta t_i \gg 1, \varepsilon \sim 10^{-3}$, the POM time-splitting scheme with forward time-averaging is either neutrally stable (without the Asselin filter), or the instability rate of SCMs is sufficiently small. The Asselin filter does not deteriorate the stability properties of the scheme.

To check the results of the numerical stability analysis we also performed a set of experiments aimed at direct stability estimates. In these experiments we solved the initial-value problem by integrating schemes (28)–(36) and (28)–(34), (37), (38) for a sufficiently long time interval (hundreds of slow mode periods). Then we computed the ratio $r = \|\boldsymbol{\psi}^{m_2}\|_E / \|\boldsymbol{\psi}^{m_1}\|_E$, where $\|\boldsymbol{\psi}^m\|_E$ denotes the energy norm of the solution on the internal time step number m. m_2 is the time step number during the last slow mode period of scheme integration with the maximum energy norm of solution (for the unstable case, m_2 is simply the last time step of scheme integration). The time step m_1 was chosen as the time step with the maximum energy norm of solution within one slow mode period in the middle of the integration time. The plots of $r^{1/(m_2 - m_1)}$ as a function of $\omega_2 \Delta t_i$ and ε (not presented here) were compared with Figs. 14 and 18. Although direct stability estimates are more noisy as compared to estimates based on the analysis of eigenvalues, a good qualitative agreement with the results of numerical stability analysis has been observed. We think that the noise is explained by the effect of rounding errors accumulating over a long integration time.

10. Conclusions

The analysis of the time-splitting procedure used in the Princeton Ocean Model (POM) has been presented. It is well known that perturbations in the ocean propagate with substantially different speeds. The procedure is aimed at developing an effective *explicit* finite-difference scheme that makes it possible to use different time steps to describe the evolution of

interacting fast and slow modes. The main idea of the procedure in the general case is to split the system of primitive equations into two systems of equations for interacting external and internal modes. The depth-integrated horizontal velocities and sea-surface height are considered the external mode while the *slow* components of the 3D-velocity vector, temperature and salinity are considered the internal mode. The external mode is governed by the depth-integrated horizontal momentum and continuity equations, in which such variables as 3D-velocity vector, temperature, and salinity are supposed to vary slowly. The internal mode is governed by the system of primitive equations, in which only the slow components of depth-integrated horizontal velocities and sea-surface height are retained. The crux of the problem is in determining a relevant filtering of fast components of these external mode variables.

Originally this POM time-splitting procedure was suggested on an heuristic level, based on some qualitative considerations. To analyze this procedure quantitatively we applied it to the simplest hydrodynamical model, having free waves with substantially different phase speeds. More precisely, we have considered the non-rotating and non-viscous two-layer model with constant depth and have applied the POM time-splitting procedure to the system of ordinary differential equations describing the evolution of amplitudes of the spatially periodic solution of equations of this model. This system has a simple exact solution helpful in estimating the accuracy of approximate solutions (Sections 2–4).

The preliminary analysis of the conventional POM time-splitting scheme with centered time-averaging demonstrated its weak instability for small values of ε typical for the deep ocean. We conducted some numerical experiments with Newtonian friction incorporated to suppress the instability of the scheme. We found that the friction needed to completely suppress the instability of scheme (28)–(36) exceeds the physically justified friction. Thus the solution of the conventional POM time-splitting scheme appears to be weakly unstable but this will manifest itself in the integration for a rather long time period only. In general, it is not easy to judge whether the total dissipation in the model is physically justified. Based on the pilot experiment, we think that in realistic applications of the POM it is useful to compare the total dissipation, especially that which is due to the Smagorinsky horizontal friction, with the dissipation caused by bottom friction. We argue that by replacing the centered time-averaging with forward time-averaging the POM time-splitting scheme would be more stable. The goal of the paper is to analyze properties of these time-splitting schemes in the case of the simplest model. We assume that questions arising in the analysis of such a model are inherent in the general model as well. At the same time, we would like to recommend against the straightforward transfer of the results obtained from the simple model to the general case. In realistic applications the stratification is not described by only one parameter ε. Moreover, our model, for example, does not take into account the possible effect of propagation of the unstable waves out of the region of interest.

We have shown that the POM time-splitting procedure has an asymptotic character with respect to a small stratification parameter ε. For a small ε typical for the deep ocean, the ratio of frequencies of slow and fast modes is $O(\varepsilon^{1/2})$. This is why all asymptotics have been considered for a small ε. But we did not restrict ourselves to the consideration of only small ε values. It was supposed that the range of admissible ε is $[1 \cdot 10^{-3}, 0.4]$. This helps to understand the behavior of the solution of the problem for the range of ε, where the slow frequency ω_2 is at least one order of magnitude smaller than the fast frequency ω_1. For the deep ocean, ε is on the order of 10^{-3}. Larger values could be typical for some motions characterized by the entrainment of water of substantially different density.

To study properties of the POM time-splitting procedure the solution of the time-split system (39)–(42) of differential equations has been examined. It was shown that the POM time-splitting scheme is viable. Formally, this system differs from original system (11)–(14) and the question is: what is the relationship between the solutions of these systems. The system (39)–(42) with the asymptotic definition of slow components provides the correct description of the slow components on a large time interval. The fast components are described correctly only on a limited time interval, which is on the order of the time period of the slow component. By and large, this conclusion is supported by the numerical analysis of the POM time-splitting finite-difference schemes.

To develop an approach to the definition of slow components similar to that used in POM, the centered, forward or backward time-averaging over some time interval T have been used. We have shown that the pure oscillatory solutions exist for centered averaging only. The forward or backward averaging give only decaying or growing oscillatory solutions, respectively. Generally speaking, the time-averaging does not provide the corresponding slow components exactly, but with some approximation only. For a very small ε, it is possible to choose a proper time-averaging interval T to provide solutions, which are close to the corresponding exact solutions. For larger ε the solutions of the time-split system of differential equations radically differ from the corresponding exact solutions of (11)–(14). This occurs despite the fact that speeds of mode propagation still differ by one order of magnitude, which makes it reasonable to apply the time-splitting procedure (Section 7).

In the next step, we applied the differential-difference approach to the analysis of time-split system of equations. Based on the substantial difference between the time steps used for the integration of the external and internal mode equations, we considered differential equations for the external mode and finite-difference equations for the internal mode. For $\omega_f \Delta t_i \gg 1$ the schemes based on centered or backward time-averaging are unconditionally unstable. The forward time-averaging provides a stable scheme under the condition that $\omega_2 \Delta t_i < 1$, where ω_2 is the slow frequency ($\omega_2 = \varepsilon^{1/2}\omega_s[1 + O(\varepsilon)]$ for small values of ε). Note that POM uses centered time-averaging. The application of the Asselin filter to schemes with centered and forward time-averaging have been considered. It appears that in both cases the filter suppresses computational modes. Yet, for the centered time-averaging, the filter does not practically modify the physical modes and the scheme remains unstable. For the forward time-averaging, the physical modes also do not change substantially and the scheme remains conditionally stable, but the instability occurs for smaller values of $\omega_2 \Delta t_i$ as compared to the case without the Asselin filter (Section 8).

Finally, the stability analysis of the POM time-splitting schemes (28)–(36) and (28)–(34), (37), (38) with and without the Asselin filter was carried out (Section 9) for high and low temporal resolution of the fast components of u_a and η and different ratios of internal and external time steps. The problem has been reduced to the study of properties of eigenvalues of some 8×8 matrix. This matrix completely describes the evolution of the solution of the finite-difference scheme. This part of the analysis has been done numerically but for the identification of eigenvalues corresponding to slow and fast computational and physical modes some analytical results were used. A set of representative cases were examined. The applicability of the differential-difference scheme outlined in Section 8 has been investigated. The analysis of the differential-difference scheme is substantially simpler compared to that of the POM finite-difference scheme (formally it implies the study of eigenvalues of a 4×4 matrix rather than a 8×8 matrix). It has been shown that the differential-difference analysis is applicable if $\omega_f \Delta t_e \ll 1$ and $\omega_f \Delta t_i \gg 1$. If these conditions are violated, the differential-difference approach may give erroneous results.

The plots of the largest modulus of eigenvalues of the appropriate matrices show that in the case of the centered time-averaging, there are practically no subregions in which this modulus is less than or equal to unity. Yet in the case with forward time-averaging such subregions exist. Thus, the scheme with centered time-averaging appears to be unconditionally unstable while the scheme with forward time-averaging appears to be conditionally stable. Details of this analysis along with a careful examination of eigenvalues for some representative examples are given in Section 9. Notice also that for very small values of ε typical for the deep ocean we did not obtain very large $|\lambda|$, so we do not foresee any 'explosive' instability of the POM time-splitting scheme with centered time-averaging for small values of ε. For larger ε an 'explosive' instability can occur (large values of $|\lambda|$).

The Asselin filter does not improve the stability of the scheme with centered time-averaging at least for small ε because for this scheme the slow physical modes are the most unstable modes. Notice that in general the instability rate grows faster than linearly with increasing $\omega_2 \Delta t_i$. That is why the common practical recommendation for the choice of Δt_i on the verge of the stability requirement ($\omega_2 \Delta t_i \sim 1$) seems to be questionable. Our analysis indicates that practically acceptable instability rates for the POM time-splitting scheme with centered time-averaging are observed if $\omega_f \Delta t_i \gg 1$ and $\omega_2 \Delta t_i \ll 1$. The POM time-splitting scheme with forward time-averaging reproduces amplitudes and phases of slow physical modes with smaller errors compared to the conventional POM time-splitting scheme with centered time-averaging. Moreover, these modes are always stable. Fast physical modes are also always stable, but the phase errors are small only if the fast mode period is well resolved ($\omega_f \Delta t_e \ll 1$). For a practically important set of parameters: $\omega_f \Delta t_e \sim 1$, $\omega_f \Delta t_i \gg 1$, $\varepsilon \sim 10^{-3}$, the POM time-splitting scheme with forward time-averaging is either neutrally stable (without the Asselin filter), or the instability rate of slow computational modes is sufficiently small. The Asselin filter does not deteriorate stability properties of the scheme.

Finally, is a proper filtering of the fast component of the external mode variables the crucial factor determining the stability of the time-splitting scheme? The common reasoning is that, in the case of improper filtering, the internal mode variables will contain the fast component, which can generate resonant growth of the external mode. Without any doubts this factor is important but there are several arguments against its crucial role. The analysis presented in Section 8 shows that the POM time-splitting scheme with centered time-averaging is unstable even if the fast mode is filtered completely in equations for the internal mode. We think that an important cause of instability in the schemes (28)–(36) and (28)–(34), (37), (38) is also a positive feedback loop which exists in the system because the internal mode variable ζ^m is taken with a lag in time with respect to external mode variables during the integration of the external mode equations. Recall also that we cannot neglect the fast component of ζ completely as has been shown in Section 6.

Acknowledgments

The authors gratefully acknowledge the support from the National Science Foundation: V. Kamenkovich through Grants OCE 96-33470 and OCE 01-18200 and D. Nechaev through Grant OCE 01-18200. This work was also supported by the National Oceanic and Atmospheric Administration grant NA06OAR4320264. We are thankful to the anonymous referees for helpful comments, as well as to David Rosenfield for his help in editing.

Appendix A. Formulas for the fast and slow components of u_a, η, u_1 and ζ for a small ε

We provide expansions in ε of the fast (superscript f) and slow (superscript s) components of u_a, η, u_1 and ζ, see (18)–(21); (26), (27). We restrict ourselves to writing out the first terms in each expansion only

$$u_a^f = -\frac{\omega_f}{Hk}\left[(a_0 + \varepsilon^{1/2} a_1 + O(\varepsilon)) e^{i\omega_f t} - (b_0 + \varepsilon^{1/2} b_1 + O(\varepsilon)) e^{-i\omega_f t}\right], \tag{A.1}$$

$$u_a^s = \varepsilon \frac{\omega_s H_2}{kH^2}\left[(c_{-1} + \varepsilon^{1/2} c_0 + O(\varepsilon)) e^{i\omega_s \varepsilon^{1/2} t} - (d_{-1} + \varepsilon^{1/2} d_0 + O(\varepsilon)) e^{-i\omega_s \varepsilon^{1/2} t}\right], \tag{A.2}$$

$$\eta^f = (a_0 + \varepsilon^{1/2} a_1 + O(\varepsilon)) e^{i\omega_f t} + (b_0 + \varepsilon^{1/2} b_1 + O(\varepsilon)) e^{-i\omega_f t}, \tag{A.3}$$

$$\eta^s = -\frac{H_2}{H}\left[(\varepsilon^{1/2} c_{-1} + O(\varepsilon)) e^{i\omega_s \varepsilon^{1/2} t} + (\varepsilon^{1/2} d_{-1} + O(\varepsilon)) e^{-i\omega_s \varepsilon^{1/2} t}\right], \tag{A.4}$$

$$u_1^f = -\frac{\omega_f}{Hk}\left[(a_0 + \varepsilon^{1/2}a_1 + O(\varepsilon))e^{i\omega_f t} - (b_0 + \varepsilon^{1/2}b_1 + O(\varepsilon))e^{-i\omega_f t}\right], \tag{A.5}$$

$$u_1^s = \frac{\omega_s}{kH_1}\left[(c_{-1} + \varepsilon^{1/2}c_0 + O(\varepsilon))e^{i\omega_s\varepsilon^{1/2}t} - (d_{-1} + \varepsilon^{1/2}d_0 + O(\varepsilon))e^{-i\omega_s\varepsilon^{1/2}t}\right], \tag{A.6}$$

$$\zeta^f = \frac{H_2}{H}\left[(a_0 + \varepsilon^{1/2}a_1 + O(\varepsilon))e^{i\omega_f t} + (b_0 + \varepsilon^{1/2}b_1 + O(\varepsilon))e^{-i\omega_f t}\right], \tag{A.7}$$

$$\zeta^s = (\varepsilon^{-1/2}c_{-1} + c_0 + \varepsilon^{1/2}c_1 + O(\varepsilon))e^{i\omega_s\varepsilon^{1/2}t} + (\varepsilon^{-1/2}d_{-1} + d_0 + \varepsilon^{1/2}d_1 + O(\varepsilon))e^{-i\omega_s\varepsilon^{1/2}t}, \tag{A.8}$$

where

$$a_j = A_j \exp\left[\left(\varepsilon i\omega_f \frac{H_2^2}{2H^2} + O(\varepsilon^2)\right)t\right], \quad b_j = B_j \exp\left[\left(-\varepsilon i\omega_f \frac{H_2^2}{2H^2} + O(\varepsilon^2)\right)t\right] \tag{A.9}$$

for $j = 0, 1, \ldots$ and

$$c_j = C_j \exp\left[\left(-\varepsilon^{3/2} i\omega_s \frac{H_2^2}{2H^2} + O(\varepsilon^{5/2})\right)t\right], \quad d_j = D_j \exp\left[\left(\varepsilon^{3/2} i\omega_s \frac{H_2^2}{2H^2} + O(\varepsilon^{5/2})\right)t\right] \tag{A.10}$$

for $j = -1, 0, 1, \ldots$. The frequencies ω_f and ω_s are given in (25).

Appendix B. Asymptotic analysis of system (39)–(42)

We apply the asymptotic method of multiple time scales (see, e.g., [12, Chapter 6]) to the analysis of system (39)–(42). According to (51)

$$\frac{d}{dt} = \frac{\partial}{\partial T_0} + \varepsilon^{1/2}\frac{\partial}{\partial T_1} + \varepsilon\frac{\partial}{\partial T_2} + \cdots \tag{B.1}$$

It is clear that u_1 and ζ will contain the slow component only so all $u_{(1)j}, j = 0, 1, \ldots$, and $\zeta_j, j = -1, 0, 1, \ldots$ will not depend on T_0. Taking this into account and using (52)–(55) yields the following equations of the first approximation,

$$\frac{\partial u_{(a)0}}{\partial T_0} = -ikg\eta_0, \tag{B.2}$$

$$\frac{\partial \eta_0}{\partial T_0} + ikHu_{(a)0} = 0, \tag{B.3}$$

$$0 = -ikg\eta_0^s, \tag{B.4}$$

$$\frac{\partial \zeta_{-1}^s}{\partial T_1} + ik(Hu_{(a)0}^s - H_1 u_{(1)0}^s) = 0. \tag{B.5}$$

The general solution of the homogeneous system (B.2), (B.3) is

$$u_{(a)0} = -\frac{\omega_f}{kH}[a_0(T_1, T_2, \ldots)e^{i\omega_f T_0} - b_0(T_1, T_2, \ldots)e^{-i\omega_f T_0}], \tag{B.6}$$

$$\eta_0 = a_0(T_1, T_2, \ldots)e^{i\omega_f T_0} + b_0(T_1, T_2, \ldots)e^{-i\omega_f T_0}, \tag{B.7}$$

where a_0 and b_0 are arbitrary functions. From (B.6) and (B.7) it follows that

$$u_{(a)0}^s = 0, \quad \eta_0^s = 0. \tag{B.8}$$

Therefore Eq. (B.4) is satisfied identically and (B.5) takes the form

$$-H_1 u_{(1)0}^s + \frac{\partial \zeta_{-1}^s}{\partial T_1} = 0. \tag{B.9}$$

The comparison of $u_{(a)0}, \eta_0$ with corresponding terms in (A.1)–(A.4) shows that they are determined correctly.

The equations of the second approximation are

$$\frac{\partial u_{(a)1}}{\partial T_0} + \frac{\partial u_{(a)0}}{\partial T_1} = -ikg\left(\eta_1 + \frac{H_2}{H}\zeta_{-1}^s\right), \tag{B.10}$$

$$\frac{\partial \eta_1}{\partial T_0} + \frac{\partial \eta_0}{\partial T_1} + ikHu_{(a)1} = 0, \tag{B.11}$$

$$\frac{\partial u_{(1)0}^s}{\partial T_1} = -ikg\eta_1^s, \tag{B.12}$$

$$\frac{\partial \zeta_0^s}{\partial T_1} + \frac{\partial \zeta_{-1}^s}{\partial T_2} + ik(Hu_{(a)1}^s - H_1 u_{(1)1}^s) = 0. \tag{B.13}$$

System (B.10) and (B.11) for $u_{(a)1}, \eta_1$ is inhomogeneous. The forcing terms in this system contain $e^{i\omega_f T_0}$ and $e^{-i\omega_f T_0}$ with some coefficients. To eliminate the resonant (secular) terms from the general solution of this system we need to put

$$\frac{\partial a_0}{\partial T_1} = 0, \quad \frac{\partial b_0}{\partial T_1} = 0. \tag{B.14}$$

Then the general solution of system (B.10) and (B.11) is

$$u_{(a)1} = -\frac{\omega_f}{kH}[a_1(T_1, T_2, \ldots)e^{i\omega_f T_0} - b_1(T_1, T_2, \ldots)e^{-i\omega_f T_0}], \tag{B.15}$$

$$\eta_1 = a_1(T_1, T_2, \ldots)e^{i\omega_f T_0} + b_1(T_1, T_2, \ldots)e^{-i\omega_f T_0} - \frac{H_2}{H}\zeta^s_{-1}, \tag{B.16}$$

where a_1 and b_1 are arbitrary functions. From (B.15) and (B.16) it follows that

$$u^s_{(a)1} = 0, \quad \eta^s_1 = -\frac{H_2}{H}\zeta^s_{-1}. \tag{B.17}$$

Substituting η^s_1 into (B.12) and invoking (B.9) we find the homogeneous system of equations for $u_{(1)0}, \zeta_{-1}$. Its general solution is

$$u^s_{(1)0} = \frac{\omega_s}{kH_1}[c_{-1}(T_2, \ldots)e^{i\omega_s T_1} - d_{-1}(T_2, \ldots)e^{-i\omega_s T_1}], \tag{B.18}$$

$$\zeta^s_{-1} = c_{-1}(T_2, \ldots)e^{i\omega_s T_1} + d_{-1}(T_2, \ldots)e^{-i\omega_s T_1} \tag{B.19}$$

where c_{-1} and d_{-1} are arbitrary functions. The comparison of $u_{(a)1}, \eta_1, u^s_{(1)0}$ and ζ^s_{-1} with corresponding terms in (A.1)–(A.8) shows that they are determined correctly.

The equations of the third approximation are

$$\frac{\partial u_{(a)2}}{\partial T_0} + \frac{\partial u_{(a)1}}{\partial T_1} + \frac{\partial u_{(a)0}}{\partial T_2} = -ikg\left(\eta_2 + \frac{H_2}{H}\zeta^s_0\right), \tag{B.20}$$

$$\frac{\partial \eta_2}{\partial T_0} + \frac{\partial \eta_1}{\partial T_1} + \frac{\partial \eta_0}{\partial T_2} + ikHu_{(a)2} = 0, \tag{B.21}$$

$$\frac{\partial u^s_{(1)1}}{\partial T_1} + \frac{\partial u^s_{(1)0}}{\partial T_2} = -ikg\eta^s_2, \tag{B.22}$$

$$\frac{\partial \zeta^s_1}{\partial T_1} + \frac{\partial \zeta^s_0}{\partial T_2} + \frac{\partial \zeta^s_{-1}}{\partial T_3} + ik(Hu^s_{(a)2} - H_1 u^s_{(1)2}) = 0. \tag{B.23}$$

First, consider the inhomogeneous system (B.20), (B.21) for $u_{(a)2}, \eta_2$. To eliminate the resonant terms we put

$$\frac{\partial a_1}{\partial T_1} + \frac{\partial a_0}{\partial T_2} = 0, \quad \frac{\partial b_1}{\partial T_1} + \frac{\partial b_0}{\partial T_2} = 0. \tag{B.24}$$

The second terms on the left-hand sides of (B.24) do not depend on T_1 (see (B.14)). Because a_1 and b_1 should be bounded, we have

$$\frac{\partial a_0}{\partial T_2} = 0, \quad \frac{\partial b_0}{\partial T_2} = 0 \tag{B.25}$$

and from (B.24)

$$\frac{\partial a_1}{\partial T_1} = 0, \quad \frac{\partial b_1}{\partial T_1} = 0. \tag{B.26}$$

The general solution of system (B.20), (B.21) is

$$u_{(a)2} = -\frac{\omega_f}{kH}[a_2(T_1, T_2, \ldots)e^{i\omega_f T_0} - b_2(T_1, T_2, \ldots)e^{-i\omega_f T_0}] - i\frac{H_2}{kH^2}\frac{\partial \zeta^s_{-1}}{\partial T_1}, \tag{B.27}$$

$$\eta_2 = a_2(T_1, T_2, \ldots)e^{i\omega_f T_0} + b_2(T_1, T_2, \ldots)e^{-i\omega_f T_0} - \frac{H_2}{H}\zeta^s_0, \tag{B.28}$$

where a_2 and b_2 are arbitrary functions. Thus

$$u^s_{(a)2} = -i\frac{H_2}{kH^2}\frac{\partial \zeta^s_{-1}}{\partial T_1}, \quad \eta^s_2 = -\frac{H_2}{H}\zeta^s_0. \tag{B.29}$$

Substituting η^s_2 into (B.22) and $u^s_{(a)1}$ (see (B.17)) into (B.13) yields the inhomogeneous system for $u^s_{(1)1}, \zeta^s_0$. The elimination of the resonant terms require that

$$\frac{\partial c_{-1}}{\partial T_2} = 0, \quad \frac{\partial d_{-1}}{\partial T_2} = 0. \tag{B.30}$$

Finally the general solution of (B.22), (B.13) is

$$u^s_{(1)1} = \frac{\omega_s}{kH_1}[c_0(T_2,\ldots)e^{i\omega_s T_1} - d_0(T_2,\ldots)e^{-i\omega_s T_1}], \tag{B.31}$$

$$\zeta^s_0 = c_0(T_2,\ldots)e^{i\omega_s T_1} + d_0(T_2,\ldots)e^{-i\omega_s T_1}, \tag{B.32}$$

where c_0 and d_0 are arbitrary functions. The comparison of $u^s_{(a)2}, \eta_2, u^s_{(1)1}$ and ζ^s_0 and derivatives of a_1, b_1, c_{-1} and d_{-1} (see (B.26) and (B.30)) with corresponding terms in (A.1)–(A.10) shows that they are determined correctly. But the similar comparison of $u^f_{(a)2}$ and derivatives of a_0, b_0 with respect to T_2 (see (B.25)) shows that they do not coincide with the corresponding terms in (A.1)–(A.10). The process of constructing and examining further approximations can be continued. It appears that all the slow components of u_a, η, u_1 and ζ are determined correctly.

Appendix C. Time averages of the external mode in differential-difference system of model equations

The solution u_a, η of (68), (69) on interval $(0, \Delta t_i)$ for $\zeta = \zeta^1$ is

$$u_a = E_1 e^{i\omega_f t} + F_1 e^{-i\omega_f t}, \tag{C.1}$$

$$\eta = -\sqrt{\frac{H}{g}}(E_1 e^{i\omega_f t} - F_1 e^{-i\omega_f t}) - \varepsilon\frac{H_2}{H}\zeta^1, \tag{C.2}$$

where constants E_1 and F_1 are easily calculated in terms of known initial conditions for u_a, η. The solution u_a, η of (68), (69) on interval $(\Delta t_i, 2\Delta t_i)$ for $\zeta = \zeta^2$ is

$$u_a = E_2 e^{i\omega_f t} + F_2 e^{-i\omega_f t}, \tag{C.3}$$

$$\eta = -\sqrt{\frac{H}{g}}(E_2 e^{i\omega_f t} - F_2 e^{-i\omega_f t}) - \varepsilon\frac{H_2}{H}\zeta^2, \tag{C.4}$$

where constants E_2 and F_2 are easily calculated from the condition of continuity of u_a and η at $t = \Delta t_i$ and so on. Further

$$\frac{1}{\Delta t_i}\int_0^{\Delta t_i} u_a\,dt = R\left(E_1 e^{\frac{1}{2}i\omega_f\Delta t_i} + F_1 e^{-\frac{1}{2}i\omega_f\Delta t_i}\right), \tag{C.5}$$

$$\frac{1}{\Delta t_i}\int_0^{\Delta t_i} \eta\,dt = -\sqrt{\frac{H}{g}}R\left(E_1 e^{\frac{1}{2}i\omega_f\Delta t_i} - F_1 e^{-\frac{1}{2}i\omega_f\Delta t_i}\right) - \varepsilon\frac{H_2}{H}\zeta^1, \tag{C.6}$$

$$\frac{1}{\Delta t_i}\int_{\Delta t_i}^{2\Delta t_i} u_a\,dt = R\left(E_2 e^{\frac{1}{2}i\omega_f\Delta t_i} + F_2 e^{-\frac{1}{2}i\omega_f\Delta t_i}\right), \tag{C.7}$$

$$\frac{1}{\Delta t_i}\int_{\Delta t_i}^{2\Delta t_i} \eta\,dt = -\sqrt{\frac{H}{g}}R\left(E_2 e^{\frac{1}{2}i\omega_f\Delta t_i} - F_2 e^{-\frac{1}{2}i\omega_f\Delta t_i}\right) - \varepsilon\frac{H_2}{H}\zeta^2, \tag{C.8}$$

where

$$R = \frac{2}{\omega_f\Delta t_i}\sin\left(\frac{\omega_f\Delta t_i}{2}\right). \tag{C.9}$$

Appendix D. Eigenvalues of matrix M in the absence of the Asselin filter for $\varepsilon = 0$

The matrix M can be represented as

$$M = \begin{pmatrix} M_e^N & M_{12} \\ M_{21} & M_{22} \end{pmatrix}, \tag{D.1}$$

where M_e, M_{12}, M_{21} and M_{22} are the 4×4 matrices, M_e^N is M_e to the power N, and M_e,

$$M_e = \begin{pmatrix} 0 & 2i\Delta t_e kg & 1 & 0 \\ 2i\Delta t_e kH & 0 & 0 & 1 \\ 1 & 0 & 0 & 0 \\ 0 & 1 & 0 & 0 \end{pmatrix}. \tag{D.2}$$

Matrix M_e^N provides changes of the external mode on the time interval of Δt_i caused by the external mode alone; matrix M_{12} provides changes of the external mode on the same time interval caused by the internal mode alone; matrix M_{21} provides changes of the internal mode caused by the external mode alone; and matrix M_{22} provides changes of the internal mode caused by the internal mode alone. It is easy to see that only matrices M_{12} and M_{22} depend on ε. For $\varepsilon = 0$ matrix $M_{12}(0)$ is equal to zero and matrix $M_{22}(0)$,

$$M_{22}(0) = \begin{pmatrix} 0 & 0 & 1 & 0 \\ 2i\Delta t_i k H_1 & 0 & 0 & 1 \\ 1 & 0 & 0 & 0 \\ 0 & 1 & 0 & 0 \end{pmatrix}. \tag{D.3}$$

It is evident now that the characteristic equation for matrix M is

$$det\{M - \lambda I\} = det\{M_e^N - \lambda I\} det\{M_{22}(0) - \lambda I\} = 0, \tag{D.4}$$

where $det\{M\}$ denotes the determinant of M, and I is the identity matrix. The characteristic equations for matrices M_e and $M_{22}(0)$ are

$$det\{M_e - \lambda I\} = (\lambda^2 - 2i\omega_f \Delta t_e \lambda - 1)(\lambda^2 + 2i\omega_f \Delta t_e \lambda - 1) = 0, \tag{D.5}$$

$$det\{M_{22}(0) - \lambda I\} = (\lambda^2 - 1)^2 = 0, \tag{D.6}$$

respectively. Thus, the eigenvalues of matrix M in the case of $\varepsilon = 0$ are (in the absence of the Asselin filter),

$$\lambda_{1,2} = \left[i\omega_f \Delta t_e \pm \sqrt{1 - (\omega_f \Delta t_e)^2} \right]^N; \quad \lambda_{3,4} = \left[-i\omega_f \Delta t_e \pm \sqrt{1 - (\omega_f \Delta t_e)^2} \right]^N, \tag{D.7}$$

$$\lambda_5 = \lambda_7 = 1; \quad \lambda_6 = \lambda_8 = -1, \tag{D.8}$$

where the superscript N in (D.7) means raising to the power of N. Note that in the case of $\varepsilon = 0$, matrix M_{21} does not influence eigenvalues (D.7) and (D.8). Therefore these eigenvalues will not change when the centered time-averaging is replaced with forward time-averaging.

References

[1] E. Anderson, Z. Bai, C. Bischof, S. Blackford, J. Demmel, J. Dongarra, J. Du Croz, A. Greenbaum, S. Hammarling, A. McKenney, D. Sorensen, LAPACK Users' Guide, third ed., Society for Industrial and Applied Mathematics, Philadelphia, PA, 1999.
[2] R. Asselin, Frequency filter for time integrations, Monthly Weather Review 100 (6) (1972) 487–490.
[3] A.F. Blumberg, G.L. Mellor, A description of a three-dimensional coastal ocean circulation model, in: N.S. Heaps (Ed.), Three Dimensional Coastal Ocean Models, American Geophysical Union, Washington, DC, 1987, pp. 1–16.
[4] S.M. Griffies, C. Böning, F.O. Bryan, E.P. Chassignet, R. Gerdes, H. Hasumu, A. Hirst, A.-M. Treguier, D. Webb, Developments in ocean climate modelling, Ocean Modelling 2 (2000) 123–192.
[5] R. Hallberg, Stable split time stepping schemes for large-scale ocean modeling, J. Comput. Phys. 135 (1997) 54–65.
[6] R.L. Higdon, A two-level time-stepping method for layered ocean circulation models, J. Comput. Phys. 177 (2002) 59–94.
[7] R.L. Higdon, Numerical modelling of ocean circulation, Acta Numer. (2006) 385–470.
[8] R.L. Higdon, A.F. Bennett, Stability analysis of operator splitting for large-scale ocean modelling, J. Comput. Phys. 123 (1996) 311–329.
[9] L.H. Kantha, C.A. Clayson, Numerical Models of Oceans and Oceanic Processes, Academic Press, 2000.
[10] P.D. Killworth, D. Stainforth, D.J. Webb, S.M. Paterson, The development of a free-surface Bryan–Cox–Semptner ocean model, J. Phys. Oceanogr. 21 (1991) 1333–1348.
[11] G.L. Mellor, Users Guide for a Three-Dimensional, Primitive Equation, Numerical Ocean Model, Program in Atmospheric and Oceanic Sciences, Princeton University Princeton, NJ, 2004. 56p.
[12] A.H. Nayfeh, Perturbation Methods, John Wiley & Sons, 1973. 425pp.